HHS Public Access

Author manuscript

Cell Metab. Author manuscript; available in PMC 2022 July 06.

Published in final edited form as:

Cell Metab. 2021 July 06; 33(7): 1449–1465.e6. doi:10.1016/j.cmet.2021.04.019.

Neurotensin is an anti-thermogenic peptide produced by lymphatic endothelial cells

Jin Li[#1,2,3,*], **Erwei Li**[#2], **Rafael S. Czepielewski**[4], **Jingyi Chi**[5], **Xiao Guo**[1], **Yong-Hyun Han**[4], **Daqing Wang**[2], **Luhong Wang**[2], **Bo Hu**[6], **Brian Dawes**[2], **Christopher Jacobs**[2], **Danielle Tenen**[2], **Samuel J. Lin**[7], **Bernard Lee**[7], **Donald Morris**[7], **Adam Tobias**[7], **Gwendalyn J. Randolph**[4], **Paul Cohen**[5], **Linus Tsai**[2,3,8], **Evan D. Rosen**[2,3,8,9,10,*]

[1]State Key Laboratory of Genetic Engineering and School of Life Sciences, Fudan University, Shanghai, China.

[2]Division of Endocrinology, Diabetes, and Metabolism, Beth Israel Deaconess Medical Center, Boston, MA

[3]Harvard Medical School, Boston, MA

[4]Department of Pathology and Immunology, Washington University School of Medicine, St. Louis, MO

[5]Laboratory of Molecular Metabolism, The Rockefeller University, New York, NY

[6]Dana-Farber Cancer Institute, Boston, MA

[7]Division of Plastic Surgery, Department of Surgery, Beth Israel Deaconess Medical Center, Boston, MA

[8]Broad Institute, Cambridge, MA

[9]Senior Author

[10]Lead Contact

[#] These authors contributed equally to this work.

SUMMARY

The lymphatic vasculature plays important roles in the physiology of the organs in which it resides, though a clear mechanistic understanding of how this cross-talk is mediated is lacking. Here, we performed single-cell transcriptional profiling of human and mouse adipose tissue and

[*]Correspondence: li_jin_lifescience@fudan.edu.cn (J.L.) or erosen@bidmc.harvard.edu (E.D.R.).

AUTHOR CONTRIBUTIONS

Conceptualization, J.L., L.T., and E.D.R.; Human Tissue Procurement, S.L., B.L., A.T., D.M.; Investigation, J.L., E.L., X.G., L.W., D.W., R.S.C., J.C., D.T., B.H., and D.P.; Analysis, J.L., C.J., B.D., and L.T.; Data Curation, L.T., B.D., and C.J.; Writing, J.L., L.T., and E.D.R.; Data Visualization, L.T., J.L., E.L., C.J., R.S.C., and J.C.; Funding Acquisition, E.D.R.; Supervision, L.T., G.J.R., P.C., and E.D.R.

DECLARATION OF INTERESTS

The authors declare no competing interests.

found that lymphatic endothelial cells highly express neurotensin (*NTS/Nts*). *Nts* expression is reduced by cold and by norepinephrine in an α-adrenergic-dependent manner, suggesting a role in adipose thermogenesis. Indeed, NTS treatment of brown adipose tissue explants reduced expression of thermogenic genes. Furthermore, adenoviral-mediated overexpression and knockdown or knockout of NTS *in vivo* reduced and enhanced cold tolerance, respectively, an effect mediated by NTSR2 and ERK signaling. Inhibition of NTSR2 promoted energy expenditure and improved metabolic function in obese mice. These data establish a link between adipose tissue lymphatics and adipocytes with potential therapeutic implications.

Graphical Abstract

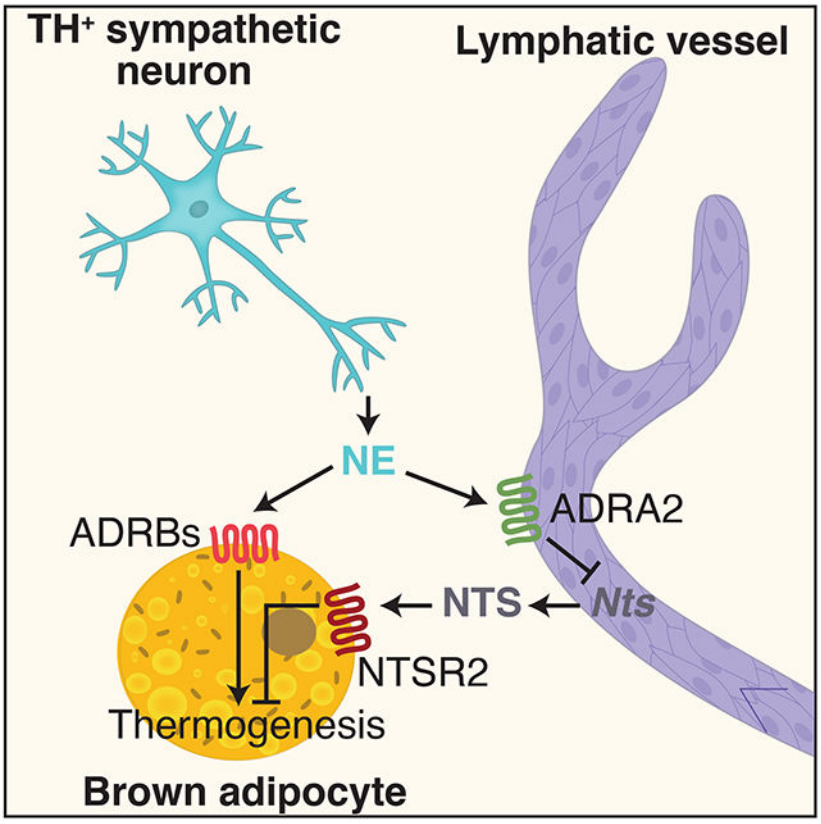

eTOC Blurb

Li et al. identify lymphatic endothelial cells as an important source of the peptide neurotensin (NTS) in adipose tissue. NTS expression and release are reduced by cold exposure and norepinephrine via the sympathetic nervous system. Once released, NTS acts to repress thermogenesis in brown adipocytes via NTSR2 signaling and ERK activation. This pathway serves as a prototype for adipose-lymphatic communication, which has significant effects on metabolic function.

Keywords

Neurotensin; lymphatic endothelial cells; adipose tissue; thermogenesis; single cell RNA-seq; NTSR2

INTRODUCTION

The lymphatic vasculature is a blind-ended network of specialized vessels that return interstitial fluid and metabolites back to the general circulation. In addition to their role in fluid homeostasis, lymphatic vessels (LVs) also transport immune cells, principally T lymphocytes and dendritic cells (DCs), from peripheral tissues to lymph nodes (Randolph et al., 2017). Lymphatic endothelial cells (LECs) are developmentally distinct from blood vessel endothelial cells and are further distinguished by the expression of specific proteins, including lymphatic vessel endothelial hyaluronan receptor-1 (LYVE1), podoplanin, neuropilin-2, vascular endothelial growth factor receptor 3 (VEGFR3; also known as Flt4) and the transcription factor prospero homeobox-1 (Prox1)(Oliver et al., 2020; Petrova and Koh, 2020).

Long thought to be passive conduits, recent evidence suggests that LVs participate actively in the function of the tissues in which they are found. This may occur by altering the tightness of the junctions between LECs, thus promoting or inhibiting fluid and cellular return (Kuan et al., 2015). In the intestine, for example, VEGF signaling induces a transition from looser “button-like” junctions between LECs to tighter “zipper-like” junctions, thus impeding the uptake of chylomicrons into the lacteals and reducing energy assimilation (Zhang et al., 2018). Another means by which LECs can regulate local tissue functions is by the elaboration of specific signaling molecules, collectively referred to as “lymphangiocrine” factors. The best-known examples are chemokines like C-C motif chemokine ligand 21 (CCL21), which is secreted by LECs and recruits lymphocytes and DCs for uptake and eventual return to local lymph nodes (Randolph et al., 2017). LECs also produce other chemokines, such as sphingosine-1 phosphate (S1P), CX3CL1 and CXCL12, especially in the setting of inflammation (Baeyens et al., 2015; Johnson and Jackson, 2013; Kabashima et al., 2007).

For many years, adipose tissue was believed to be devoid of lymphatic drainage, but recent studies have identified LVs within the parenchyma of adipose tissue, particularly in the mesenteric fat (Escobedo and Oliver, 2017). Interestingly, it is now clear that there is bidirectional cross-talk between lymphatics and adipose tissue (Escobedo and Oliver, 2017; Ivanov et al., 2016; Rosen, 2002). Obesity impairs lymphatic function in humans and mice, and adiposity is an independent risk factor for lymphedema (Savetsky et al., 2014; Swenson et al., 2009; Weitman et al., 2013). Conversely, lymphatic dysfunction promotes deposition of fat, as seen in both human patients and animal models of lymphedema (Harvey et al., 2005; Rutkowski et al., 2010; Tavakkolizadeh et al., 2001). At present there is little understanding of the mechanistic underpinnings of these interactions.

We have performed single-cell RNA-seq (scRNA-seq) of the stromal-vascular fraction from both mouse and human adipose tissue. Among the many cell types identified were LECs,

which express the expected markers (e.g. *Prox1, Lyve1*), but which also express a gene (*NTS/Nts*) that encodes the common precursor for two peptides, neuromedin N and neurotensin (NTS). Neurotensin is a multifunctional 13 amino acid peptide expressed highly in the brain and in specific enteroendocrine cells (Tyler-McMahon et al., 2000). NTS has potent anti-nociceptive properties (Kleczkowska and Lipkowski, 2013), and it has been observed to cause reduced food intake, in which context it is being explored as a weight loss therapy (Fredrickson et al., 2014). These data predict that mice lacking NTS would be obese, but in fact, the opposite is true; $Nts^{-/-}$ mice are highly resistant to the adverse effects of high fat feeding, an effect attributed to reduced intestinal lipid absorption (Li et al., 2016).

We observed that *Nts* expression in adipose LECs is reduced by cold exposure and norepinephrine, an effect mediated by α_2-adrenergic receptor signaling. This pattern of thermal regulation in adipose tissue suggested that NTS might play an inhibitory role in adaptive thermogenesis, which has been proposed as a therapeutic avenue in obesity and other metabolic diseases (Harms and Seale, 2013). Using an array of gain- and loss-of-function studies *in vivo* and *ex vivo*, we show that NTS does, in fact, reduce adaptive thermogenesis in brown adipocytes. Furthermore, we demonstrate that NTSR2 mediates the anti-thermogenic and obesity-promoting actions of NTS, providing an opportunity for the development of selective therapeutics targeting this system.

RESULTS

scRNA-seq of mouse adipose SVF identifies numerous cell types

In a chow-fed mouse, adipocytes make up roughly half of the cells in a fat pad, depending on the depot (Roh et al., 2017). To assess the diversity of non-adipocyte cell types, we performed scRNA-seq of the stromal-vascular fraction (SVF) of multiple adipose depots in mice. Epididymal and inguinal white adipose tissue (eWAT and iWAT, respectively) and interscapular brown adipose tissue (BAT) was harvested from 8 week old chow-fed male C57Bl/6J mice. Adipocytes were separated from SVF by collagenase digestion and low speed centrifugation, after which pelleted cells were subjected to droplet-based scRNA sequencing. Overall, approximately 22,000 unique cells were sequenced and analyzed. Cells were classified into several distinct clusters, most of which were easily identifiable by defined marker expression, including preadipocytes, mesothelial cells, macrophages, monocytes, B lymphocytes, T lymphocytes, NK cells, and vascular cells (Figs. 1A, B).

Subclustering of vascular cells within mouse and human adipose SVF

We next focused specifically on vascular cells within the adipose tissue, a relatively understudied population relative to preadipocytes and immune cells. Subclustering of murine vascular cells revealed eight distinct populations (labeled MmV1-8), including five clusters of endothelial cells and three clusters of mural cells (Fig. 1C). Clusters of endothelial cells could be assigned to venule or capillary cells (V1; expressing *Timp4* and *Car4*), arteriolar cells (V2; expressing *Sema3g* and *Hey1*), stalk cells (V3; expressing *Selp, Lrg1, Plvap*, and *Ackr1*), tip cells (V4; expressing *Fscn1* and *Patchd4*), and LECs (V5; expressing *Prox1* and *Pard6g*)(Fig. 1D)(Chen et al., 2019; Kutschera et al., 2011; Li et al., 2019; Vanlandewijck et al., 2018; Zhao et al., 2018). All clusters were represented in every depot tested, although

some cell types exhibited differential enrichment. For example, LECs were more likely to be found in eWAT than in iWAT or BAT, while arteriolar ECs showed the opposite pattern (Fig. 1E).

We also performed a similar analysis of approximately 27,000 SVF cells from human subcutaneous adipose tissue. The vascular fraction of these cells was resolved into six clusters, including four endothelial cell subtypes and two mural populations (Fig. S1A,B). Combining the human and murine vascular data enabled increased power to detect new cellular features, causing a new subcluster to emerge from the venule-capillary group, which we identify as fenestrated capillary cells, expressing *Plvap* and *Lrg1* but not *Selp* or *Ackr1* (Fig. S1C-E) (Li et al., 2019; Stan et al., 2012).

Lymphatic endothelial cells express *Nts*

LECs were easily identified in both species and all depots tested, based on the presence of known markers, such as *Lyve1, Prox1*, and *Flt4*. Among the unique markers seen in both human and murine LECs, we noted the presence of *NTS/Nts* (Fig. 2A, B). This gene, hereafter referred to by its mouse name *Nts*, encodes two peptides, neurotensin and neuromedin N. Neurotensin is a pleiotropic 13-amino acid peptide produced by the brain and by specialized neuroendocrine cells in the gut (Tyler-McMahon et al., 2000). *Nts* expression was not evenly distributed among all LECs. Rather, there was segregation of *Nts* and *Lyve1* expression, noted especially in the human data (Fig. S2A-C). Given that *Lyve1* is known to preferentially mark lymphatic capillaries (Randolph et al., 2017), this suggested that *Nts* might be most highly expressed in lymphatic collecting vessels, at least in humans.

To further investigate the expression of *Nts* in LVs, we took advantage of the Nts-Cre mouse, which expresses Cre recombinase downstream of an IRES sequence in the 3' UTR of the *Nts* locus (Leinninger et al., 2011). Crossing these mice to the Ai9 tdTomato reporter line (Madisen et al., 2010) marks cells that express or have expressed the *Nts* gene. Mesenteric fat from Nts-Cre::Ai9 mice was isolated and tdTomato was visualized by immunofluorescence. tdTomato fluorescence was seen in both lymphatic capillaries (Fig. 2C, D) and in collecting vessels, particularly in and around the valves. Counterstaining for the canonical lymphatic markers Lyve1 and Prox1 confirmed that the bulk of tdTomato was in LVs, although NTS-Cre also marks blood capillaries to a small degree (Fig. 2C, D). This was not seen in the scRNA-seq data, and so could represent either very low level NTS expression in these cells or possibly prior NTS expression earlier in the developmental lineage of blood ECs.

We next isolated GFP+ cells by flow sorting from the epididymal fat of Nts-Cre::NuTRAP mice, which express GFP in an Nts-Cre-dependent manner (Roh et al., 2017). qRT-PCR analysis revealed that *Nts, Flt4, Reln, Prox1*, and *Pard6g* were enriched in GFP+ vs GFP− cells, demonstrating that Nts-Cre is marking LECs as predicted (Fig. 2E). We then performed the converse experiment, crossing Prox1-CreERT2 to Ai9 mice and treating with tamoxifen. We isolated the tdTomato+ cells from the epididymal fat of these mice and assessed expression of *Prox1* and *Reln*, which were highly enriched, demonstrating that the LECs of these mice were labeled with tdTomato as expected. These cells also expressed *Nts*,

thus providing an orthogonal line of evidence that LECs do, in fact, express this gene (Fig. 2F).

To ensure that NTS protein is made by LECs, we isolated BAT from NTS-Cre mice and transduced it ex vivo with AAV9-DIO-hM3Dq, which expresses the DREADD hM3Dq in a Cre-dependent manner. The hM3Dq modified muscarinic receptor activates Gq signaling, which in this setting will mimic α1-adrenergic receptor signaling (Docherty, 2019). As shown below, α1-adrenergic agonist causes a significant induction of *Nts* expression. Addition of the DREADD ligand CNO elicited the secretion of Nts into the media, as determined by ELISA (Fig. S2D). We also isolated individual lymphatic collecting ducts from human mesenteric fat and showed that lysates contain the proneurotensin protein (Fig. S2E, F).

Finally, we asked whether *Nts* is expressed exclusively in LECs from adipose tissue, or whether this is a general feature of LECs. We first took advantage of the Immgen database (www.immgen.org), which houses RNA-seq data from many immunological tissues, including lymph nodes. Querying the Immgen database clearly identified *NTS* expression in LECs from lymph nodes, as well as in thymic epithelium (Fig. S2G). We next used our Nts-Cre::Ai9 mice to examine LVs in other tissues. We observed intense tdTomato fluorescence in intestinal lacteals (Fig. S2H), as well as in the lymphatic vasculature of the ear (Fig. S2I) and diaphragm (Fig. S2J), indicating that *Nts* expression is a general property of lymphatics throughout the body.

Nts expression in lymphatic endothelial cells is repressed by sympathetic stimulation

We were interested to test whether *Nts* expression is regulated by physiological conditions. We first examined BAT, iWAT, and eWAT SVF from animals housed under thermoneutral (30°C) or cold (4°C) conditions. *Nts* mRNA levels were highest in BAT SVF, followed by iWAT and then eWAT (Figs. 3A, S3A). In all three depots, cold exposure was associated with significantly reduced *Nts* expression. Furthermore, NTS protein was markedly lower in BAT after 1 day of cold exposure (Fig. 3B). We inferred that this must reflect *Nts* expression in LECs, as our scRNA-seq data indicate that this is the only cell population in the fat pad to express this gene. To confirm this, we isolated adipose LECs from warm (30°C) and cold (4°C) Prox1-tdTomato mice, and again found that cold exposure was associated with significantly lower *Nts* expression in this highly purified cell type without altered expression of other LEC genes (Figs. 3C, S3B).

Information about ambient temperature is conveyed to BAT by the sympathetic nervous system (SNS), which releases norepinephrine at bouton-like projections that comprise the “neuro-adipose junction” (Zeng et al., 2015). Norepinephrine then activates β-adrenergic receptors on the surface of the adipocyte to induce a broad array of responses that promote thermogenesis. We speculated that norepinephrine, delivered by the SNS, might also drive the reduction of *Nts* expression in LECs. There are several studies that demonstrate a physical and functional connection between the SNS and LVs (see Discussion for details); none of these studies have been performed in adipose tissue, however. To address this, we first assessed the physical proximity of sympathetic nerves and LVs in fat. Prox1-CreERT2 mice were crossed to Ai9 reporter mice and treated with tamoxifen to label LECs and then

imaged after tissue clearing. We noted close apposition of tyrosine hydroxylase (TH)-positive nerve fibers (as a marker of the SNS) **[AU: correct as edited? YES]**with Prox1+ lymphatics in epididymal, inguinal, and brown adipose tissue depots (Figs. S3C-E). We next isolated SVF from BAT and cultured it *ex vivo*. Treatment of these cells with 1 and 5 uM norepinephrine caused a dose-dependent reduction in *Nts* expression (Fig. 3D). Because this result could be seen if norepinephrine was killing or otherwise injuring the LECs in the culture, we looked at another LEC-specific gene (*Prox1*) and found that it was not reduced by norepinephrine treatment (and was in fact induced) (Fig. 3D). To demonstrate that this effect is truly occurring in LECs, we again isolated tdTomato+ cells from the BAT of Prox1-tdTomato mice; treatment of these cells with norepinephrine had the same effect on *Nts* expression seen in the SVF as a whole (Fig. 3E).

Because norepinephrine activates both α- and β-adrenergic receptors, we tested the effect of selective adrenergic agonists and antagonists on the ability of norepinephrine to repress *Nts* expression. As shown in Fig. S3F, the non-specific α-adrenergic blocker phentolamine prevented the actions of norepinephrine on *Nts* mRNA levels, while the β-adrenergic antagonist propranolol did not. Furthermore, stimulation with the α_1-adrenergic agonist phenylephrine did not decrease *Nts* (and in fact significantly induced its expression), but the α_2-agonist dexmedetomidine had the same effect as norepinephrine (Fig. S3G). Taken together, these pharmacological studies indicate that sympathetic stimulation suppresses *Nts* levels in brown adipose LECs via α_2-adrenergic signaling.

Thus far, we showed that physical proximity exists between sympathetic nerves and LVs in adipose tissue, and that direct stimulation of LECs with norepinephrine reduces NTS expression. These data suggest, but do not prove, the existence of an SNS→LEC axis in adipose tissue. To demonstrate that, we drove sympathetic stimulation of BAT in living mice, and measured the effect on *Nts* expression in adipose LECs. The neurocircuitry of sympathetic outflow to BAT is known: thermal sensory inputs are integrated in the preoptic area and dorsal medial hypothalamus, which then activate Vglut3+ premotor neurons in the raphe pallidus (RPa). These glutamatergic neurons activate preganglionic neurons in the intermediolateral (IML) nucleus of the spinal cord, which drive activation of the sympathetic ganglion neurons that innervate BAT (Francois et al., 2018) (Fig. 3F). We performed stereotaxic injections into the RPa of 6-8-week-old male Vglut3-IRES-Cre::Prox1-tdTomato mice with AAV2/8-hSyn-DIO-hM3Dq-mCherry, forcing the expression of the DREADD hM3Dq specifically in glutamatergic neurons. Following a 3-week recovery period, mice received IP injection of CNO (1 mg/kg) or saline, and BAT was harvested 3 hours later. c-Fos immunohistochemistry of the RPa after CNO confirmed that Vglut3 neurons were activated as expected (Fig. S3H), and elevated *Ucp1* expression in BAT indicated successful activation of the sympathetic outflow to BAT (Fig. 3G). As predicted, *Nts* mRNA and NTS protein levels were lower in BAT in the CNO-treated mice in a DREADD-dependent manner compared to the controls (Figs. 3H, I).

NTS is anti-thermogenic

Regulation of *Nts* expression by temperature and norepinephrine suggested that NTS might play a role in adipose thermogenesis, specifically as an anti-thermogenic factor. We tested

this first using BAT explants *ex vivo*. Addition of NTS in increasing amounts led to a dose-dependent lowering of UCP-1 protein compared to the untreated control cells (Fig. 4A). This was not due to death of the cells, as adiponectin expression was not affected by NTS treatment. At the mRNA level, NTS treatment at 2 doses (25 and 50 μM) resulted in lower nuclear expression of thermogenic and mitochondrial genes compared to control treatments (Fig. 4B). Similar results were seen in cultured thermogenic adipocytes differentiated from BAT SVF *ex vivo* (not shown). These cells were also assessed for oxygen consumption after NTS administration, and demonstrated a lower degree of basal, uncoupled, and maximal respiration (Fig. 4C).

We next tested the effect of NTS *in vivo*. NTS has an extremely short serum half-life in rodents (approximately 30 seconds; (Aronin et al., 1982)), making direct administration difficult. We therefore opted to generate an AAV construct that overexpresses the full length pro-NTS. This AAV (or a GFP-expressing control AAV) was injected directly into the BAT of wild-type C57Bl/6J mice, and BAT was harvested one week later. Treatment with the AAV-NTS resulted in higher local expression of *Nts* mRNA (by 15-fold) compared to treatment with AAV-GFP (Fig. 4D), accompanied by significantly lower expression of several thermogenic genes (Fig. 4E). UCP-1 protein levels were lower as well (Fig. 4F). This had physiological consequences, as AAV-NTS injected mice were less tolerant of an acute cold challenge (Fig. 4G), and their BAT contained more lipid, consistent with lower intrinsic thermogenic activity, relative to mice that received AAV-GFP (Fig. 4H). As predicted, indirect calorimetry revealed that mice exhibited significantly lower energy expenditure, O_2 consumption, and CO_2 production at 4°C (Figs. 4I, S4A, B). Of note, the reduction in energy expenditure in mice receiving AAV-NTS appeared to be smaller than might be predicted by the reduction in UCP-1 protein; this may reflect UCP-1 independent pathways, e.g., shivering.

Lymphatic endothelial release is responsible for the anti-thermogenic actions of NTS

Our studies indicate that NTS has anti-thermogenic properties, but they do not prove that lymphatic-derived NTS is a physiological regulator of thermogenesis. To address this, we took three orthogonal approaches. First, we crossed Prox1-CreERT2 mice to RC::L-hM3Dq (Jax 026943) mice, which express the DREADD hM3Dq and mCherry in a Cre-dependent manner. We treated Prox1-CreERT2::DREADD and DREADD only (Cre−) mice with tamoxifen and then harvested the BAT. LVs were properly targeted, as evidenced by co-localization of mCherry and Lyve-1 in BAT (Fig. S4C). When CNO was added to the medium, NTS protein was released in Cre+ BAT explants only (Fig. S4D), which resulted in lower *Ucp1* mRNA and protein (Figs. S4E, F). This result demonstrates that forced NTS release from endogenous LECs in BAT results in reduced thermogenic gene expression.

Next, we performed a loss-of-function study *in vivo* using an AAV that expresses a short hairpin RNA directed against endogenous *Nts* (shNTS). Direct injection of AAV-shNTS into the BAT of wild-type mice at thermoneutrality (30°C) resulted in lower levels of *Nts* mRNA by 50% relative to mice that received an AAV with a scrambled control shRNA (Fig. 5A). Thermogenic gene expression and UCP-1 protein levels were higher in mice receiving AAV-shNTS (Fig. 5B, C). We also noted that the typical “whitened” appearance of BAT at

thermoneutrality was restored to a histological appearance more typical of room temperature, with reduced lipid content (Fig. 5D). Mice receiving AAV-shNTS were better able to defend their core temperature in the face of an acute cold challenge following a shift from thermoneutrality relative to mice that received the control shRNA (Fig. 5E). Because LECs are the only source of NTS within BAT, this demonstrates that lymphatic NTS is required for the anti-thermogenic effect.

To address this further, we also generated *Nts*^{flox} mice (Fig. 6A), and crossed them to Prox1-CreERT2 mice to create mice where the *Nts* allele is ablated specifically in LECs. Following tamoxifen treatment, these mice displayed lower *Nts* expression in BAT (Fig. 6B). As predicted, they also exhibit higher thermogenic gene expression and UCP-1 protein levels in BAT at thermoneutrality relative to tamoxifen-treated Cre^{-} mice (Figs. 6C, D). Finally, these LEC-specific NTS KO mice display lower BAT lipid content at 30°C, and they are more cold tolerant than control mice (Figs. 6E, F). Taken together, our data demonstrate that LEC-derived NTS is an endogenous regulator of BAT thermogenesis.

The anti-thermogenic effect of NTS is mediated by NTSR2 and ERK signaling

NTS is known to interact with three distinct receptors, including two G protein coupled receptors (NTSR1 and NTSR2) and the type I membrane glycoprotein sortilin (Sort1, also called NTSR3). Because the functional relevance of sortilin in plasma membrane-based NTS signal transduction is unclear, we focused on *Ntsr1* and *Ntsr2*. We first queried our prior RNA-seq data of gene expression in isolated brown, beige, and white adipocytes (Roh et al., 2018) and found that *Ntsr2* is expressed in all three adipocyte types, while *Ntsr1* was not detected (Fig. 7A). We therefore tested whether loss of NTSR2 function would enhance thermogenesis in BAT. Viral delivery of a specific short hairpin knocked down *Ntsr2* expression by ~75% in BAT (Fig. 7B). This was associated with higher thermogenic gene expression and UCP-1 protein levels relative to mice that received an AAV expressing a scrambled control shRNA (Fig. 7C, S5A). Concordant with this, BAT that received shNtsr2 was less lipid-filled at 30°C (Fig. S5B), and those mice were better able to withstand a cold challenge than control mice (Fig. 7D).

The signal transduction mechanisms used by NTSR2 are incompletely understood, and studies in different tissues and physiological contexts suggest there can be context-dependent variability (Mazella and Vincent, 2006). NTSR2 activates ERK1/2 signaling in several different cell types, so we assessed that in cultured thermogenic adipocytes. In these cells, NTS treatment led to higher ERK1/2 phosphorylation in a dose- and time-dependent fashion relative to vehicle-treated cells (Figs. S5C, D). Furthermore, the MEK inhibitor PD0325901 blocked NTS-mediated repression of UCP-1 mRNA and protein expression, providing direct evidence of MAP kinase pathway involvement (Figs. S5E, F).

The *Nts* gene encodes the precursor protein for both NTS and the six amino acid peptide Neuromedin N (NN) (Fig. S6A). The receptor for NN is unclear, but there are some reports that it may signal via NTSR2 (Gendron et al., 2004; Toth et al., 2016). Given this, we sought to determine whether NN could account for any of the phenotype seen when the entire NTS sequence is targeted. To that end, we treated cultured brown adipocytes directly with purified

NN. This did not cause activation of ERK (Fig. S6B), nor did it affect thermogenic gene expression or UCP-1 protein levels in these cells (Figs. S6C, D).

Pharmacological blockade of NTSR2 induces thermogenesis and prevents further weight gain in obese mice

In order to determine whether the NTS-NTSR2 signaling axis could be targeted therapeutically, we used NTRC-824, an NTSR2-specific small molecule inhibitor (Thomas et al., 2016). As before, NTS treatment of cultured brown adipocytes resulted in higher pERK levels, and this effect was markedly attenuated if NTRC-824 was added simultaneously (Fig. S6E, F). Similarly, the lower thermogenic gene expression in BAT explants caused by NTS treatment was reversed by NTRC-824 (Fig. S6G). We extended this line of investigation into the in vivo setting by administering NTRC-824 directly to mice (5 mg/kg IP) for 14 days at 30°C. This caused induction of thermogenic gene and UCP-1 protein expression, and also resulted in lower lipid content in BAT relative to vehicle-treated mice (Figs. 7E, S6H, I). Mice receiving NTRC-824 were better able to defend their core body temperature during an acute cold challenge (Fig. 7F). Finally, mice treated with NTRC-824 displayed higher energy expenditure and body temperature by indirect calorimetry (Figs. 7G, S6J).

Finally, we asked whether longer term treatment with NTRC-824 might have beneficial effects on metabolism in an obese mouse model. Mice were made obese by high fat feeding (with 60 kcal% fat) for 12 weeks and then treated with NTRC-824 (5 mg/kg IP) for 1 month. Animals treated with vehicle continued to gain weight over the course of the experimental period, while those receiving NTRC-824 were resistant to further weight gain (Fig. S7A). NTRC-824 treated mice had lower adiposity despite no change in food intake, as well as improved glucose and insulin tolerance (Figs. S7B-F). As expected, NTRC-824 resulted in higher thermogenic gene expression in BAT and improved BAT histology at 30°C (Figs. S7G, H).

DISCUSSION

The lymphatic system has long been viewed as a passive set of conduits that enable the recapture of interstitial fluid for eventual return to the circulation, and as a passage for lymphocytes to the lymph nodes. This now appears to be a gross oversimplification, as there is burgeoning evidence that LVs participate actively in the functions of the tissues they drain. One of the best examples of this is in the intestine, where LVs can respond to secreted signals to alter their permeability, and thus contribute to the regulation of nutrient absorption (Zhang et al., 2018). There are also well-established links between lymphatic vasculature and local immunity, coordinated in part by LEC-mediated secretion of cytokines and chemokines like CCL19, CCL21, S1P, CX3CL1 and CXCL12 (Brown et al., 2018; Johnson and Jackson, 2010; Mendoza et al., 2017; Zhuo et al., 2012). The secretion of EGF and PDGF-BB from LECs can also promote tumor cell proliferation and neoangiogenesis in a breast cancer model (Lee et al., 2014). More recently, LECs were shown to elaborate the protein reelin, which has profound effects on cardiac growth (Liu et al., 2020).

There is evidence for significant cross-talk between lymphatics and adipose tissue. For example, there are numerous studies that demonstrate that excess adiposity has adverse effects on lymphatic integrity, density, contractility and flow, and that these effects are reversible with weight loss (Blum et al., 2014; Garcia Nores et al., 2016; Hespe et al., 2016; Nitti et al., 2016; Savetsky et al., 2014). Conversely, primary defects in lymphatic function can lead to increased adiposity. For example, patients with secondary lymphedema from disruption of LVs accumulate adipose tissue, particularly in regions directly in contact with lymphatic fluid (Escobedo and Oliver, 2017; Rosen, 2002; Tavakkolizadeh et al., 2001). The same can be seen in various mouse models of lymphatic dysfunction, including Vegf3 and Prox1 mutants, where adipose tissue accumulates near areas of leaking lymphatic fluid, and also more generally to cause obesity (Harvey et al., 2005; Karkkainen et al., 2001; Rutkowski et al., 2010). Despite the depth of these connections, virtually nothing is known about the mechanistic underpinnings by which lymphatics contribute to metabolic homeostasis.

Our scRNA-seq data from adipose SVF revealed that LECs express the neuropeptide *Nts*. We went on to show that NTS protein is released by LECs, and that expression of *Nts* is seen in LECs throughout the body. In adipose tissue LECs, *Nts* expression is regulated by temperature and by norepinephrine in a manner that suggested that it might act as an anti-thermogenic agent. We show that this is, in fact, the case, using a variety of genetic and pharmacological models. NTS works on thermogenic adipocytes via the NTSR2-MAP Kinase pathway.

Our study is not the first to demonstrate a direct connection between the sympathetic nervous system and lymphatics. A histological (Alessandrini et al., 1981) and pharmacological (McHale et al., 1980) relationship between SNS neurons and LVs was demonstrated as far back as the early 1980s. Norepinephrine was also shown to stimulate lymphatic contractility in bovine mesentery and canine thoracic duct, which could be blocked by the α-adrenergic antagonists phentolamine and phenoxybenzamine (McHale et al., 1979; Russell et al., 1980). A direct connection to the SNS was demonstrated by showing that electrical stimulation of the lumbar sympathetic chain increased lymphatic contractility and lymph flow, an effect which could also be blocked by phentolamine (McGeown et al., 1987). More recently, chronic stress was shown to cause remodeling of the lymphatic vasculature around tumors in an SNS-dependent manner, with implications for tumor progression and metastasis (Le et al., 2016). We show here that there is close apposition of TH+ sympathetic nerves and LVs in adipose depots, and that norepinephrine exerts a negative effect on NTS production. This action of norepinephrine can be blocked by α-adrenergic, but not β-adrenergic, antagonists. Although we do not know how the LEC parses the actions of norepinephrine on multiple adrenergic receptors, our pharmacological data indicates that α2-adrenergic receptors are the primary mediators of the *Nts*-reducing effect of norepinephrine. Taken together, our data suggest a model in which sympathetic stimulation induces thermogenesis in two ways: through a direct pathway mediated by β-adrenergic activation of adipocytes themselves and also via an indirect pathway mediated by α-adrenergic repression of NTS in adipose lymphatics. We do not yet know whether this response to norepinephrine is seen in LECs outside of adipose tissue.

Given that NTS expression is a feature of LECs throughout the body, it is likely that this neuropeptide plays roles in the lymphatic system beyond regulation of thermogenesis, though direct evidence for this is scant. NTS injection into the popliteal lymph nodes of sheep caused a sharp reduction in the efflux of lymphocytes from the node (Moore, 1984). There are also data suggesting that NTS (via NTSR1) affects the initiation, progression and metastasis of many different types of cancer (Alifano et al., 2010; Allen et al., 1988; Dupouy et al., 2009; Souaze et al., 2006; Su et al., 2019; Wang et al., 2011). Future studies should be undertaken to elucidate the effect of NTS on lymphatic permeability, contractility and flow.

When we manipulate the *Nts* gene, we are affecting both known cleavage products, NTS and NN. Assays for NN are not readily available, and little is known about its downstream actions. Our experiments using purified NTS on BAT explants and cultured adipocytes indictate that the NTS peptide has anti-thermogenic properties. It is possible that NN also contributes to the effects that we see *in vivo*, such as when we selectively knockout the Nts gene in LECs.

There are three known NTS receptors: the G protein coupled receptors NTSR1 and NTSR2, and the type I membrane glycoprotein sortilin (SORT1; also called NTSR3) (Mazella et al., 1998). Of the first two, we only detect expression of NTSR2 in adipocytes, which led us to hypothesize that this receptor mediates the anti-thermogenic actions of NTS. Interestingly, NTSR1 has been reported to be expressed in adipocytes that have been exposed to 2,4,6,-trinitrobenzensulphonic acid (TNBS), an experimental inducer of inflammation in colon and mesenteric fat (Koon et al., 2009). It is therefore possible that NTS signals through NTSR1 in adipocytes under certain conditions, particularly those that promote inflammatory changes. SORT1, on the other hand, is highly expressed in adipocytes, among many other tissues (Lin et al., 1997; Morris et al., 1998). Most SORT1 is associated with intracellular membranes, such as the endoplasmic reticulum and the Golgi network, although approximately 10% of Sort1 protein is located on the plasma membrane (Mazella et al., 1998) where it binds NTS as well as other neuroactive peptides (Munck Petersen et al., 1999; Quistgaard et al., 2009). We did not test whether an interaction with SORT1 participates in the anti-thermogenic response to NTS, but we note that inhibition of NTSR2 either by knockdown or by the small molecule NTRC-824 enhances thermogenesis to the same extent as knockdown of the ligand NTS. This suggests that NTSR2 is the dominant NTS receptor on adipocytes in the context of energy expenditure.

There are a few studies using artificial systems (e.g. CHO or COS cells overexpressing human NTSR2) suggesting that NTS unexpectedly acts as an antagonist of NTSR2 signaling (Richard et al., 2001; Vita et al., 1998). Other studies have not reproduced these findings, however, and have consistently shown that NTS is an agonist of NTSR2, even in some of the same heterologous systems tested earlier (Botto et al., 1998; Gendron et al., 2004; Mazella et al., 1996; Sarret et al., 2002). Studies *in vivo* have been more consistent, clearly demonstrating that NTS acts as an agonist of NTSR2. For example, NTS acts as an agonist on NTSR2 in the brains of mice and rats (Steele et al., 2017; Tabarean, 2020). Similarly, NTRC-824, was originally reported as an agonist of NTSR2 in a FLIPR-based calcium release assay in CHO cells (Thomas et al., 2014). The same group later showed that *in vivo*, NTRC-824 is an NTSR2 antagonist (Thomas et al., 2016). This is consistent with our own

data showing that NTRC-824 blocks the actions of exogenous NTS and phenocopies knockdown of NTSR2 in vivo.

The signal transduction mechanism of NTSR2 is not completely elucidated and may be highly dependent on the cellular context (Mazella and Vincent, 2006), but it has been proposed that NTS induces the internalization of NTSR2, and this in turn promotes the activation of ERK1 and ERK2 (Gendron et al., 2004). Although some MAP kinases, such as p38, are critical for *Ucp1* expression and subsequent brown fat activity (Cao et al., 2001; Robidoux et al., 2005), ERK1/ERK2 have been proposed to inhibit UCP1 in the context of IGF1 signaling (Porras et al., 1998). Similarly, TNF-α reduces *Ucp1* expression in an ERK-dependent manner (Valladares et al., 2001). Given these data, we tested the role of ERK signaling in the anti-thermogenic actions of NTS, and demonstrated that ERK is activated by NTS in brown adipocytes. We also found that the selective MEK inhibitor PD0325901 blocks the actions of NTS on *Ucp1* mRNA levels. Taken together, our data suggest that NTS inhibits thermogenesis via NTSR2-mediated activation of ERK1/2.

Interestingly, NTS is being explored as an anti-obesity agent, primarily on the basis of its anorexigenic effects. NTS reduces food intake when injected ICV or in specific brain regions (Beck et al., 1998; Cooke et al., 2009). The effects of peripheral NTS administration have been harder to demonstrate, in large part because of its very short serum half-life (~30 seconds in rodents)(Aronin et al., 1982). This obstacle has been overcome by the administration of PEGylated NTS, which improves stability 10-fold; PEGylated NTS delivered to the peripheral circulation diminishes appetite and promotes weight loss in obese rodents (Ratner et al., 2019; Ratner et al., 2016). This effect is in seeming opposition to our finding that NTS is anti-thermogenic, and that NTSR2 antagonism promotes increased energy expenditure and weight loss in obese mice. These data may be reconciled by the fact that the anorexigenic actions of NTS are mediated through NTSR1. Mice lacking NTSR1 exhibit increased food intake and body weight (Remaury et al., 2002), and the administration of exogenous NTS does not induce hypophagia in these mice (Woodworth et al., 2017). Furthermore, leptin injection is less efficacious in reducing food intake in NTSR1 null mice (Kim et al., 2008). NTS thus can both promote and oppose weight gain through different mechanisms in different tissues.

Of significant interest in this regard is the reported observation that mice lacking NTS globally ($Nts^{-/-}$) are lean and protected from the adverse consequence of high fat feeding (Li et al., 2016); this finding was associated with reduced intestinal absorption of lipid in an NTSR1 and NTSR3 dependent manner. Heterozygous KO mice were not examined. Homozygous null mice exhibited a small reduction (rather than the expected increase) in food intake; no change in energy expenditure was detected. It is difficult to reconcile the data from $Nts^{-/-}$ mice, which reflect the actions of NTS in multiple tissues integrated over the development and lifetime of the animal, with the observed role of NTS as an anorexigenic agent and as a suppressor of thermogenesis as demonstrated here. Nonetheless, the data suggest that the anabolic actions of NTS (which would include promotion of intestinal lipid absorption as well as anti-thermogenesis) are dominant. It is also worth pointing out that lipid absorption in the intestine is a function of the local LVs, called lacteals. Reduced absorption of lipid in the intestine of $Nts^{-/-}$ mice was suggested to occur

as a result of the missing NTS from neuroendocrine cells of the gut (Li et al., 2016); our data suggests that local effects of LEC-produced NTS may also play a role in this effect.

Finally, recent epidemiological data support an association between serum pro-NTS levels and adverse metabolic outcomes in human subjects. Pro-NTS represents the stable uncleaved pro-protein from which NTS is derived; its levels were positively correlated with incident Type 2 diabetes and with cardiovascular disease and mortality in the Malmo Diet and Cancer Study (Melander et al., 2012). Similar results were seen in the Framingham Heart Study cohort, in which subjects in the highest quartile of pro-NTS were heavier with a higher waist circumference, and higher risk of cardiovascular disease and diabetes (Januzzi et al., 2016). More recently, higher serum pro-NTS was shown to correlate with the incidence and severity of nonalcoholic fatty liver disease (Barchetta et al., 2018b) and with increased visceral adipose inflammation, a marker of the dysmetabolic state (Barchetta et al., 2018a). These associations are consistent with the idea that NTS may generally act to promote weight gain, possibly due to inhibition of adipose thermogenesis.

Limitations of the Study

Our studies in BAT explants used pharmacological doses of NTS to repress thermogenic gene expression. Reassuringly, however, our DREADD-based gain-of-function (which releases endogenous NTS) and our loss-of-function studies *in vivo* demonstrate that NTS is a physiological regulator of adipose thermogenesis. Although many models were used in this study to show that NTS represses thermogenesis, we only tested whether this action had effects on weight gain using one model, involving the small molecule NTSR2 antagonist NTRC-824. Many of our other models employed transient overexpression or knockdown of NTS/NTSR2, and such manipulations are not suitable for long-term high fat feeding studies. In addition, the relationship between brown fat activation, thermogenesis and resistance to weight gain is already well established in rodents. Our studies do not address questions about heterogeneity of the NTS response; one might expect that adipocytes closest to LVs might be more lipid filled and express less UCP-1. In our histological analysis, we do not see such patchiness. Finally, when considering our lymphatic-specific NTS knockout model, we cannot preclude the possibility that the Prox1-CreERT2 allele may express in Prox1+ cells in gut, brain or elsewhere. This is why we used orthogonal approaches that do not rely on Prox1-CreERT2 to demonstrate that lymphatic NTS is both necessary and sufficient to inhibit thermogenesis. Nonetheless, our data do not preclude the possibility that NTS from non-lymphatic sources might contribute to the anti-thermogenic effects that we observe.

STAR★METHODS

RESOURCE AVAILABILITY

Lead Contact—Requests for reagents and resources should be directed to the Lead Contact, Evan Rosen (erosen@bidmc.harvard.edu).

Materials Availability—All unique/stable reagents generated in this study are available from the Lead Contact with a completed Materials Transfer Agreement. *NTS*$^{-/-}$ mice are being deposited at Jackson Labs.

Data and Code Availability—Single-cell RNA-seq data has been deposited to the Single Cell Atlas at the Broad Institute https://singlecell.broadinstitute.org/. Mouse adipose SVF data is at:

https://singlecell.broadinstitute.org/single_cell/study/SCP708/mouse-adipose-stromal-vascular-fraction:

Human adipose SVF data is at:

https://singlecell.broadinstitute.org/single_cell/study/SCP133/human-adipose-svf-single-cell. Code to reproduce clustering data may be found on GitHub, here: https://github.com/rosen-lab/sc-svf-nts.

EXPERIMENTAL MODEL AND SUBJECT DETAILS

Animals—All animal experiments were performed according to procedures approved by the BIDMC Institutional Animal Care and Use Committee and/or the Animal Ethics Committee of Fudan University. Mice were maintained under a 12 hr light/12hr dark cycle at constant temperature (23°C) with free access to food and water. Mice were deemed to be healthy at all times and were under the care of an on-site veterinarian. Wild-type C57B6/J mice were obtained from Jackson Laboratory and used for experiments after an acclimatization period of several weeks. Experiments involving lymphatic NTS KO mice used littermate controls. All animal studies were performed at least twice on independent cohorts. For studies in lean animals, 8-10 week old male mice were used. The chow diet used was from Harlan Teklad (catalog #8664; 12.5% kcal from fat); high fat diet came from Research Diets (catalog #D12492i; 60 % kcal from fat). To label NTS expressing cells, NuTRAP mice (Roh et al., 2017)(Jax 029899) or Ai9(RCL-tdT) mice (Jax 007909) were crossed with NTS-Cre (Jax 017525). To label lymphatic endothelial cells, Ai9(RCL-tdT) mice were crossed with Prox1-Cre-ERT2 (Jax 022075). Other mouse strains used include: Vglut3-IRES-Cre (Zeng et al., 2019) and RC::L-hM3Dq (Jax 026943). *Nts*^{flox} mice were generated using CRISPR-Cas9. Two guide RNAs (GCCACAGAGATACCCCGTGGA, TCTAAGGATAACTTGAGAAT) flanking the fourth exon of *Nts* were synthesized by PNA-BIO. The guide RNAs, the single-stranded DNA repair template (synthesized by Genewiz) and Cas9 enzyme (PNA-BIO, CP01) were microinjected together into fertilized eggs of mice of the FVB/NJ background at the transgenic core of Beth Israel Deaconess Medical Center. F1 progeny were genotyped with the following primers: TCTGATGGTGCCTTCCCTCT, GCTGAAGAGGACGACACGTAAA. The wild-type allele yielded a band of 181 bp and the Nts-floxed allele yielded a band of 215bp. F1 progeny carrying the *Nts*^{flox} allele were then backcrossed to C57BL/6J mice purchased from Jackson Laboratory for 10 generations to create congenic mice. Progeny carrying the *Nts*^{flox} allele were then crossed to Prox1-CreERT2 (Jax 022075) mice to generate lymphatic endothelial cell-specific *Nts* knockout mice. *Nts*^{flox} mice have been submitted to Jackson Labs for distribution (Jax#036262).

Human Samples—Periumbilical adipose tissue samples were obtained from subjects undergoing panniculectomy, abdominoplasty, or unilateral breast reconstruction using periumbilical tissue at Beth Israel Deaconess Medical Center under IRB protocol 2011P000079. Written informed consent was obtained from each individual (n = 11)

donating tissue and samples were anonymized and handled according to the ethical guidelines set forth by the BIDMC Committee on Clinical Investigations. Subjects were recruited from the plastic surgeon operating room schedule at BIDMC in a consecutive fashion, as scheduling permitted. The inclusion criteria were healthy female subjects, >18 years old receiving abdominal surgery. Subjects taking insulin-sensitizing medications such as thiazolidinediones or metformin, chromatin-modifying drugs such as valproic acid, and drugs known to induce insulin resistance such as mTOR inhibitors (for example, sirolimus or tacrolimus) or systemic steroid medications were excluded. Any patient with breast cancer had localized disease and were >12 months removed from any chemotherapy or radiation treatments. The samples were verified as tumor free by gross pathological assessment prior to dissociation and by single-cell sequencing. BMI measures were derived from electronic medical records and confirmed by self-reporting. For other experiments, human mesenteric adipose tissue fixed in formalin was collected after pathology sign-out from trauma-associated resections and used to dissect out mesenteric adipose lymphatic vessels under IRB protocol 201111038 from Washington University School of Medicine in St. Louis.

METHOD DETAILS

Mouse SVF isolation—Epididymal, inguinal, and interscapular brown adipose tissue was dissected from 8-10 week old C57/Bl6J male mice, minced, and digested in PBS with 10 mg/ml BSA and 1 mg/mL collagenase (Worthington, CLSAFB) for 40 min at 37°C. The digested solution was filtered through a 100 um cell strainer, centrifuged at 800 rpm for 5 min and the red blood cells were lysed by ACK buffer (Thermo Fisher). The stromal-vascular fraction (SVF) pellet was then suspended in the appropriate buffer for next use; this was DMEM medium with 10% FBS and 1% P/S for cell culture experiments. All primary cells used were from male C57Bl/6 mice. All cell culture was performed at 5% CO_2, 37°C.

Purification of human SVF—Whole-tissue subcutaneous adipose specimens were freshly collected from the operating room. Skin was removed, and adipose tissue was cut into 1-2 inch pieces and rinsed thoroughly with 37°C PBS to remove blood. Cleaned adipose tissue pieces were quickly minced with an electric grinder with 3/16-inch hole plate, and 400 ml of sample was placed in a 2L wide-mouthed Erlenmeyer culture flask with 100 ml of freshly prepared blendzyme (Roche Liberase TM, research grade, cat. no. 05401127001 at a ratio of 6.25 mg per 50 ml PBS) and shaken in a 37°C shaking incubator at 120 r.p.m. for 15–20 min to digest until the sample appeared uniform. Digestion was stopped with 100 ml of freshly made KRB (5.5 mM glucose, 137 mM NaCl, 15 mM HEPES, 5 mM KCl, 1.25 mM $CaCl_2$, 0.44 mM KH_2PO_4, 0.34 mM Na_2HPO_4 and 0.8 mM $MgSO_4$), supplemented with 2% BSA. Digested tissue was filtered through a 300-μM sieve and washed with KRB/albumin until only connective tissue remained. Sample was divided into 50ml conical tubes and were centrifuged at 233 x g for 5 min at room temperature. Floating adipocytes and clear lipid from lysed adipocytes were removed by pipette, and SVF fractions were combined and subjected to RBC lysis using ACK lysis buffer (Thermo Fisher, cat no. A1049201) per manufacturer instructions.

Drop-seq—Drop-seq was performed as described (Macosko et al., 2015), with the following modifications: first, flow rates of 2.1 mL/h were used for each aqueous suspension and 12 mL/h for the oil. Second, libraries were sequenced on the Illumina NextSeq500, using between 1.6-1.7 pM in a volume of 1.2 mL HT1 and 3 mL of 0.3 μM Read1CustSeqB (GCCTGTCCGCGGAAGCAGTGGTATCAACGCAGAGTAC) using 20 x 8 x 60 read structure. Sequencing, Drop-seq read alignment and generation of digital expression data was performed through the Boston Obesity and Nutrition Center Functional Genomics Core.

Raw sequence data was first filtered to remove all read pairs with a barcode base quality of less than 10. The second read (60bp) was then trimmed at the 5′ end to remove any TSO adaptor sequence and at the 3′ end to remove poly(A) tails of length 6 or greater, then aligned to the mouse (mm10) genome using STAR v2.6.1e with default settings. Uniquely mapped reads were grouped by cell barcode. To digitally count gene transcripts, a list of UMIs in each gene, within each cell, was assembled. unambigously-related UMIs within an edit distance of 1 of one another were merged together. The total number of UMI sequences was counted, and this number was reported as the number of transcripts of that gene for a given cell. All cells containing at least 400 transcripts and having less than 10% mitochondrial gene expression were used in downstream analysis resulting in a 69,407 barcode data set (46,607 from human cells; 22,800 from mouse).

Single-Cell Clustering and Analysis—Doublets from multiple cell types were detected within the processed data using the scrublet program (Wolock et al., 2019) on a per-sample basis. Using a doublet score of 0.25 as cutoff, 674 cells were subsequently excluded from the mouse SVF data, and 1447 cells were excluded from the human SVF data. Further analyses were conducted using the Seurat program (v3.0.3.9036)(Stuart et al., 2019). For quality control, we removed genes which were expressed in fewer than 2 cells, and cells for which fewer than 400 UMIs or greater than 10% mitochondrial gene reads were were detected. Simultaneous data normalization/scaling and variable feature detection was performed using SCTransform (Hafemeister and Satija, 2019). Cells were clustered via Seurat's shared nearest neighbor clustering algorithm ("FindNeighbors" and "FindClusters") using the cthe top 50 PCs and a resolution of 0.1 (mouse) and 0.4 (human). The clustering was visualized using Uniform Manifold Approximation and Projection (UMAP)(Becht et al., 2018). Cluster markers were obtained with the Seurat function "FindMarkers" using default settings (Wilcoxon rank-sum test, min. log fold-change >= 0.25, min. fraction of cells >= 10%). Sub-clustering analysis of mouse vascular cells was performed as above, with the following additions. Cells were integrated by depot using canonical correlation analysis (CCA)(Butler et al., 2018) following recommended practices for Seurat integration with SCTransform (https://satijalab.org/seurat/v3.0/integration.html). The top 35 most variable PCs were used for subsequent clustering. Human and mouse vascular data were integrated by species as above, using homologous gene sets.

Western Blotting—For explant samples, the interscapular brown fat pads were dissected, minced and exposed to different chemicals with indicated concentration. For tissue samples, the interscapular brown fat pads were dissected and snap-frozen with liquid nitrogen. The samples were homogenized in 1% NP40 buffer with protease inhibitors with metal beads in

a Qiagen TissueLyser II (85300). Lysates were then separated by SDS-PAGE and transferred to Immobilon P membranes (Millipore). For the human collecting vessel immunoblots, human mesenteric collecting lymphatic vessels from formalin-fixed tissues were carefully isolated from the adipose tissue using fine forceps. After isolation, vessels were stabilized by incubation in PAXgene Tissue Stabilization buffer (PreAnalytiX) for at least 3 hr at room temperature. The protein lysates were extracted by homogenization in Extraction EXB buffer (Qiagen). Western blotting was conducted as described above using specific antibodies against UCP-1 (1:1000), ADIPOQ (1:1000), ERK (1:1000), pERK (1:1000), pro-NTS (1:600) and PROX1 (1:1000). SignalFire™ ECL Reagent (Cell Signaling) was used for visualization of protein bands.

Whole Mount Immunofluorescence—Different adipose depots were fixed in a 4% paraformaldehyde and 30% sucrose solution overnight at 4°C. Tissues permeabilized in PBS with 1% BSA, 1% Triton X-100 and 5% Donkey Serum overnight at 4°C, and then incubated with primary antibodies (Lyve1: 1/600, Prox1: 1/500) containing 0.1% Triton X-100 overnight at 4°C , in a rotor shaker. Samples were washed with PBS, and incubated with secondary antibodies at room temperature for 1-2 h. After washing, tissue was cleared as descripted before (Randolph et al., 2016). Briefly, tissue transparency was achieved by dehydration with 50%, 70% and 100% graded step of 30 minutes of ethanol solutions and incubation with methyl salicylate overnight. Images were collected using Leica SP8 confocal microscope and image analysis was performed with Imaris x64.

Adipo-Clear—Adipo-Clear was performed as described (Chi et al., 2018a; Chi et al., 2018b). Briefly, mice were heavily anesthetized with an overdose of isofluorane and an intracardiac perfusion and fixation was performed with 1xPBS followed by 4% PFA. All harvested samples were post-fixed in 4% PFA at 4°C overnight. Fixed samples were washed in PBS for 1 hr three times, then washed in 20%, 40%, 60%, 80% methanol in H_2O/0.1% Triton X-100/0.3 M glycine (B1N buffer, pH 7), and 100% methanol for 30 min each. Sample were then delipidated with 100% dichloromethane (DCM; Sigma-Aldrich) for 30 min three times. After delipidation, samples were washed in 100% methanol for 30 min twice, then in 80%, 60%, 40%, 20% methanol in B1N buffer for 30 min each step. All procedures above were carried out at 4°C with shaking. Samples were then washed in B1N for 30 min twice followed by PBS/0.1% Triton X-100/0.05% Tween 20/2 mg/ml heparin (PTwH buffer) for 1hr twice before further staining procedures.

For immunolabeling, samples were incubated in primary antibody dilutions in PTxwH for 4 days. After primary antibody incubation, samples were washed in PTxwH for 5 min, 10 min, 15 min, 30 min, 1 hr, 2 hr, 4 hr, and overnight, and then incubated in secondary antibody dilutions in PTxwH for 4 days. Samples were finally washed in PTwH for 5 min, 10 min, 15 min, 30 min, 1 hr, 2 hr, 4 hr, and overnight. In this study, RFP (1:200, Rockland, cat# 600-401-379) and TH (1:200, Millipore, AB1542) were used. Secondary antibodies conjugated with Alexa-568 and Alexa-647 were purchased from Invitrogen (1:200).

Samples were dehydrated in 25%, 50%, 75%, 100%, 100% methanol/H2O series for 30 min at each step at RT. Following dehydration, samples were washed with 100% DCM for 30

min twice, followed by an overnight clearing step in dibenzyl ether (DBE; Sigma-Aldrich). Samples were stored at RT in the dark until imaging.

All whole-tissue samples were imaged on a light-sheet microscope (Ultramicroscope II, LaVision Biotec) equipped with 1.3X (used for whole-tissue views with low-magnification) and 4X objective lenses (used for high-magnification views) and an sCMOs camera (Andor Neo). Images were acquired with the ImspectorPro software (LaVision BioTec). Samples were placed in an imaging reservoir filled with DBE and illuminated from the side by the laser light sheet. The samples were scanned with the 488, 561, and 640nm laser channels and with a step-size of 4 mm for 1.3x objective and 2.5 mm for 4x objective.

All whole-tissue images were generated using Imaris x64 software (Bitplane). 3D reconstruction was performed using the “volume rendering” function. Optical slices were obtained using the “orthoslicer” tool. 3D pictures and optical sections were generated using the “snapshot” tool.

AAV injection—AAV particles were ordered from Applied Biological Materials. Analgesics was administrated 16 hours prior and after injection. 8-10-week-old mice were anesthetized with Isoflurane. Hair was removed from the interscapular area using clippers followed by a surgical scrub alternating between Iodophor and 70% alcohol. A small cut was made to the skin with surgical scissors to expose the interscapular BAT. 5 μl of NTS-AAV, NTS-shRNA-AAV or NTSR2-shRNA-AAV (Serotype 8, 10^9GC/ml) was slowly injected into each lobe of the BAT using a 10 μl-Hamilton syringe. GFP-AAV or scrambled shRNA-AAV was used as control, respectively. The skin was closed with 9mm autoclips. The autoclips were removed 1 week after injection. Experiments were performed 2-4 weeks after injection.

Body Composition—Body composition to determine lean mass and fat mass values were obtained prior to the experiment with Echo MRI (Echo Medical Systems, Houston, Texas) using a 3-in-1 Echo MRI Composition Analyzer. No significant differences in body mass or composition were observed for this experiment between groups.

Indirect Calorimetry with Cold Exposure—Indirect calorimetry was performed using Comprehensive Lab Animal Monitoring System (CLAMS, Columbus Instruments; Columbus, OH, USA) housed within a temperature-controlled environmental chamber at BIDMC. 16 male C57Bl/6J mice at 8-10 weeks of age were purchased from Jackson Laboratory and injected intraperitoneally daily in the afternoon. Mice 1-8 were injected with vehicle, 9-16 with the Neurotensin Receptor Antagonist, NTRC-824 (5 mg/kg). All animals underwent surgeries to implant temperature probes (G2 E-Mitter, Starr Lifescience) within the peritoneal cavity. Two weeks after surgery, the mice were housed in the CLAMS with the light photoperiod matching that of the vivarium, 6am-6pm. All mice were provided ad libitum access to Labdiet 5008 chow (56.5/17/26.5 carbohydrate/fat/protein) throughout the experiment. Mice were maintained at 23°C for 3 days prior to 4°C over 3 hr. Mice were kept at 4°C for 12 hr which coincided with the dark photoperiod from 6pm-6am. Three mice failed to mount an adaptive response to the cold challenge and were rescued in accordance with IACUC directives. These included 1 mouse from the control group and 2 from the

NTRC-824 treated group; the partial data collected from these animals was included until the time of rescue. Statistical analysis was performed with CalR (Mina et al PMID: 30017358).

Cold challenge—Male C57BL/6J mice housed at 30°C were fed chow diet with free access to water and food for 2-3 weeks. Mice were then moved to 4°C for the indicated length of time. Core body temperature was measured using a rectal probe (Yellow Spring Instruments).

Glucose and insulin tolerance testing—For the glucose tolerance test, mice were fasted overnight and 1g/kg glucose was administered i.p. Blood samples were collected and glucose levels were determined with a portable glucometer at 0, 15, 30, 60, 90, and 120 minutes. For the insulin tolerance test, mice were fasted for 5 hours and 0.8 U/kg insulin was administered i.p. Blood glucose levels were measured at 0, 15, 30, 60, 90, and 120 minutes.

Stereotaxic surgery and viral injections—Mice were anesthetized with a ketamine (100 mg kg−1) and xylazine (10 mg kg−1) cocktail diluted in 0.9% saline, and then mounted in a stereotaxic apparatus (David Kopf model 940). An incision was made to expose the skull and a small craniotomy (coordinate AP/DV/ML: −5.8/−5/0 mm) was made through the skull for virus injection. AAV (50 nL) was injected slowly (20 nL/min) into the medullary raphe via a glass pipette (20–40 μm diameter tip) by an air pressure system (Clippard EV 24VDC). The glass pipette was left in place for five minutes after injection and then slowly withdrawn. The incision was secured using Vetbond tissue adhesive (3M). Subcutaneous injection of sustained release Meloxicam (4 mg kg−1) was provided as postoperative care. The AAV2/8-hSyn-DIO-hM3Dq-mCherry (Addgene plasmid 44361; donating investigator, Dr. Bryan Roth) was packaged at BIDMC. The control virus AAV2/5-hSyn-DIO-mCherry was ordered from Penn Vector Core (Addgene plasmid 50459). To enable recovery and AAV expression, mice were housed for a minimum of 21 days following virus injection. Accuracy of AAV injections was confirmed via post-hoc histological analysis of mCherry fluorescent protein reporters. All subjects determined to be surgical “misses” based on little or absent reporter expression were removed from analyses.

Chemogenetic activation of raphe pallidus—To activate raphe neurons, Saline- or CNO (Sigma, C0832)-loaded minipumps (Braintree scientific, AP-1007D) were implanted subcutaneously to deliver saline or CNO into mice at a constant rate of 0.5ug/hr. 3 days later, BAT was collected and homogenized in a dounce homogenizer in PBS. The homogenate was centrifuged at 12,000g for 15 minutes. The fat layer was removed and the supernatant was saved for NTS measurement by ELISA.

Chemogenetic activation of BAT LECs—AAV9-DIO-hM3Dq was injected into the BAT of Prox1-CreERT2 mice, which were then injected with Tamoxifen (75mg/kg body weight) for 11 consecutive days to induce recombination. Twenty-one days after viral injection, BAT was dissected, chopped into small pieces (approximately 0.5mm in diameter), and cultured in DMEM (Thermo Fisher 11885084). After overnight CNO stimulation (100uM), media were collected and NTS protein levels were determined by ELISA.

Medium was collected and centrifuged at 12,000g for 15 minutes. The supernatant was saved for NTS measurement by ELISA and BAT explants were used to determine the mRNA level of Ucp1 and Nts by qRT-PCR. DREADD expression in BAT LECs was confirmed by histological analysis of mCherry fluorescent protein reporters.

Tissue H&E staining—Tissues were fixed in 10% formalin. Paraffin-embedding, sectioning and Hemotoxylin and Eosin staining were performed by the BIDMC histology core facility. Histochemical staining of tissues was visualized with an EVOS microscope using a 10x objective lens.

NTRC-824 Injection—8-week-old lean male mice or 20-week-old obese mice received intraperitoneal (IP) injections of NTSR2 inhibitor NTRC-824 (5 mg/kg) (R&D Systems) or DMSO control in sterile PBS every day while housed at 30°C. The mice were treated for two weeks (lean mice) or four weeks (obese mice) and various assays were performed during the treatment. At the end of the experiment, the interscapular brown fat pads were collected and stored for later analysis.

RNA Isolation/Quantitative RT-PCR—TRIzol (Thermo Fisher) was used for total tissue and explant RNA isolation. Qiagen Micro RNeasy kit was used for SVF and lymphatic endothelial cell RNA isolation. Extracted RNA (500ng) was converted into cDNA using the PrimeScript™ RT reagent Kit (Takara). Quantitative RT-PCR (qRT-PCR) was performed using an Applied Biosystems QuantStudio 5 and SYBR Green PCR Master Mix (Applied Biosystems). Fold change was determined by comparing target gene expression with the reference gene *36b4*. All qRT-PCR assays utilized 2-4 technical replicates for each sample, and were performed using two biological replicates.

Cell purification—SVF from adipose tissue of NTS-cre::NuTRAP, NTS-cre::tdTomato or Prox1− CreERT2::tdTomato was isolation as described above. The cells were suspended by PBS with 1% BSA and filtered through 10mm cell strainers. Resuspended nuclei were sorted using a BD FACS Aria II, gating on FSC, SSC, GFP and DsRED fluorescence in BIDMC FACS core facility. To perform cell culture afterwards, the cells were sorted in DMEM medium with 10% FBS and 1% P/S. To perform RT- qRT-PCR, the cells were sorted directly into TRIzol.

Cellular respiration assay—Adipocytes differentiated from inguinal WAT SVF cells of C57BL/6J mice were plated in the poly-D-lysine coated XF96 plate in extracellular flux assay media (non-buffered DMEM containing 10 mM glucose, 4 mM L-glutamine, and 2 mM sodium pyruvate). Oxygen consumption rate (OCR) and extracellular acidification rate (ECAR) were measured using the mitochondrial stress test procedure for basal OCR followed by sequential addition of 3.5 mM oligomycin (Calbiochem), 1 mM fluoro-carbonyl cyanide phenylhydrazone (FCCP) (Enzo) and 14 mM rotenone/14 mM antimycin A (Enzo) with the XF96 Extracellular Flux Analyzer (Seahorse Bioscience).

Stimulation of LECs and SVF with adrenergic agonists and antagonists.—SVF cells were purified by modified Rodbell method and LECs were purified based on combination of tdTomato (Prox1) positive and CD45 negative signals using FACS. Cells

were cultured for 16 hours before NE or agonist/antagonist treatment. NE was made as a 10 mM stock in DMSO stock and diluted into medium at the doses indicated in the figures. Treatment was extended for 48 hours prior to cell harvest. Phentolamine and propranolol were used at a final concentration of 10uM, while phenylephrine and dexmedetomidine were used at 5uM.

QUANTIFICATION AND STATISTICAL ANALYSIS

Wild-type mice were randomly assigned to treatment groups. No animal experiment was blinded. Sample sizes were based on a combination of estimation of effect sizes in mnetabolic research and the number of available mice of the appropriate genotype and sex. All data in this study were normally distributed, and no datapoints were excluded from analysis. Methods for statistical analysis of the single-cell RNA-seq data is presented in the Methods above. Energy expenditure was calculated with ANCOVA using total mass as the covariate at each time point. Similar results were observed using lean body mass as the covariate. Body temperature changes were similarly analyzed with ANOVA. Other assays were analyzed using standard *t*-testing with statistical parameters indicated in figure legends.

ADDITIONAL RESOURCES

None.

Supplementary Material

Refer to Web version on PubMed Central for supplementary material.

ACKNOWLEDGEMENTS

This work was supported by NSFC 32071138 and MOST 2020YFA0803600 to J.L., FA-2020-01-IBD-1 to R.S.C., NIH R01 DK120649 to P.C., DOD W81XWH-15-1-0251 and NIH 2P30DK057521 to L.T., NIH R01 DK119147 and DP1 DK1109668 to G. J. R., and RC2 DK116691, R01 DK085171, R01 DK102173, R01 DK102170, and R01 DK1113669 to E.D.R. We thank the BNORC supported Functional Genomics and Bioinformatics Core and the Energy Homeostasis Core at the BIDMC, particularly Yuchen He, June Corrigan, and Alex Banks.

REFERENCES

Alessandrini C, Gerli R, Sacchi G, Ibba L, Pucci AM, and Fruschelli C (1981). Cholinergic and adrenergic innervation of mesenterial lymph vessels in guinea pig. Lymphology 14, 1–6. [PubMed: 7289657]

Alifano M, Souaze F, Dupouy S, Camilleri-Broet S, Younes M, Ahmed-Zaid SM, Takahashi T, Cancellieri A, Damiani S, Boaron M, et al. (2010). Neurotensin receptor 1 determines the outcome of non-small cell lung cancer. Clin Cancer Res 16, 4401–4410. [PubMed: 20810387]

Allen AE, Carney DN, and Moody TW (1988). Neurotensin binds with high affinity to small cell lung cancer cells. Peptides 9 Suppl 1, 57–61. [PubMed: 2856809]

Aronin N, Carraway RE, Ferris CF, Hammer RA, and Leeman SE (1982). The stability and metabolism of intravenously administered neurotensin in the rat. Peptides 3, 637–642. [PubMed: 7134032]

Baeyens A, Fang V, Chen C, and Schwab SR (2015). Exit Strategies: S1P Signaling and T Cell Migration. Trends Immunol 36, 778–787. [PubMed: 26596799]

Barchetta I, Cimini FA, Capoccia D, Bertoccini L, Ceccarelli V, Chiappetta C, Leonetti F, Di Cristofano C, Silecchia G, Orho-Melander M, et al. (2018a). Neurotensin Is a Lipid-Induced

Gastrointestinal Peptide Associated with Visceral Adipose Tissue Inflammation in Obesity. Nutrients 10.

Barchetta I, Cimini FA, Leonetti F, Capoccia D, Di Cristofano C, Silecchia G, Orho-Melander M, Melander O, and Cavallo MG (2018b). Increased Plasma Proneurotensin Levels Identify NAFLD in Adults With and Without Type 2 Diabetes. J Clin Endocrinol Metab 103, 2253–2260. [PubMed: 29590379]

Becht E, McInnes L, Healy J, Dutertre CA, Kwok IWH, Ng LG, Ginhoux F, and Newell EW (2018). Dimensionality reduction for visualizing single-cell data using UMAP. Nat Biotechnol.

Beck B, Stricker-Krongrad A, Richy S, and Burlet C (1998). Evidence that hypothalamic neurotensin signals leptin effects on feeding behavior in normal and fat-preferring rats. Biochem Biophys Res Commun 252, 634–638. [PubMed: 9837758]

Blum KS, Karaman S, Proulx ST, Ochsenbein AM, Luciani P, Leroux JC, Wolfrum C, and Detmar M (2014). Chronic high-fat diet impairs collecting lymphatic vessel function in mice. PLoS One 9, e94713. [PubMed: 24714646]

Botto JM, Chabry J, Sarret P, Vincent JP, and Mazella J (1998). Stable expression of the mouse levocabastine-sensitive neurotensin receptor in HEK 293 cell line: binding properties, photoaffinity labeling, and internalization mechanism. Biochem Biophys Res Commun 243, 585–590. [PubMed: 9480852]

Brown M, Johnson LA, Leone DA, Majek P, Vaahtomeri K, Senfter D, Bukosza N, Schachner H, Asfour G, Langer B, et al. (2018). Lymphatic exosomes promote dendritic cell migration along guidance cues. J Cell Biol 217, 2205–2221. [PubMed: 29650776]

Butler A, Hoffman P, Smibert P, Papalexi E, and Satija R (2018). Integrating single-cell transcriptomic data across different conditions, technologies, and species. Nat Biotechnol 36, 411–420. [PubMed: 29608179]

Cao W, Medvedev AV, Daniel KW, and Collins S (2001). beta-Adrenergic activation of p38 MAP kinase in adipocytes: cAMP induction of the uncoupling protein 1 (UCP1) gene requires p38 MAP kinase. J Biol Chem 276, 27077–27082. [PubMed: 11369767]

Chen W, Xia P, Wang H, Tu J, Liang X, Zhang X, and Li L (2019). The endothelial tip-stalk cell selection and shuffling during angiogenesis. J Cell Commun Signal 13, 291–301. [PubMed: 30903604]

Chi J, Crane A, Wu Z, and Cohen P (2018a). Adipo-Clear: A Tissue Clearing Method for Three-Dimensional Imaging of Adipose Tissue. J Vis Exp.

Chi J, Wu Z, Choi CHJ, Nguyen L, Tegegne S, Ackerman SE, Crane A, Marchildon F, Tessier-Lavigne M, and Cohen P (2018b). Three-Dimensional Adipose Tissue Imaging Reveals Regional Variation in Beige Fat Biogenesis and PRDM16-Dependent Sympathetic Neurite Density. Cell Metab 27, 226–236 e223. [PubMed: 29320703]

Cooke JH, Patterson M, Patel SR, Smith KL, Ghatei MA, Bloom SR, and Murphy KG (2009). Peripheral and central administration of xenin and neurotensin suppress food intake in rodents. Obesity (Silver Spring) 17, 1135–1143. [PubMed: 19214175]

Docherty JR (2019). The pharmacology of alpha1-adrenoceptor subtypes. Eur J Pharmacol 855, 305–320. [PubMed: 31067439]

Dupouy S, Viardot-Foucault V, Alifano M, Souaze F, Plu-Bureau G, Chaouat M, Lavaur A, Hugol D, Gespach C, Gompel A, et al. (2009). The neurotensin receptor-1 pathway contributes to human ductal breast cancer progression. PLoS One 4, e4223. [PubMed: 19156213]

Escobedo N, and Oliver G (2017). The Lymphatic Vasculature: Its Role in Adipose Metabolism and Obesity. Cell Metab 26, 598–609. [PubMed: 28844882]

Francois M, Qualls-Creekmore E, Berthoud HR, Munzberg H, and Yu S (2018). Genetics-based manipulation of adipose tissue sympathetic innervation. Physiol Behav 190, 21–27. [PubMed: 28859876]

Fredrickson P, Boules M, and Richelson E (2014). Neurotensin agonists in the regulation of food intake. Int J Obes (Lond) 38, 474. [PubMed: 23860334]

Garcia Nores GD, Cuzzone DA, Albano NJ, Hespe GE, Kataru RP, Torrisi JS, Gardenier JC, Savetsky IL, Aschen SZ, Nitti MD, et al. (2016). Obesity but not high-fat diet impairs lymphatic function. Int J Obes (Lond) 40, 1582–1590. [PubMed: 27200507]

Gendron L, Perron A, Payet MD, Gallo-Payet N, Sarret P, and Beaudet A (2004). Low-affinity neurotensin receptor (NTS2) signaling: internalization-dependent activation of extracellular signal-regulated kinases 1/2. Mol Pharmacol 66, 1421–1430. [PubMed: 15361549]

Hafemeister C, and Satija R (2019). Normalization and variance stabilization of single-cell RNA-seq data using regularized negative binomial regression. Genome Biol 20, 296. [PubMed: 31870423]

Harms M, and Seale P (2013). Brown and beige fat: development, function and therapeutic potential. Nat Med 19, 1252–1263. [PubMed: 24100998]

Harvey NL, Srinivasan RS, Dillard ME, Johnson NC, Witte MH, Boyd K, Sleeman MW, and Oliver G (2005). Lymphatic vascular defects promoted by Prox1 haploinsufficiency cause adult-onset obesity. Nat Genet 37, 1072–1081. [PubMed: 16170315]

Hespe GE, Kataru RP, Savetsky IL, Garcia Nores GD, Torrisi JS, Nitti MD, Gardenier JC, Zhou J, Yu JZ, Jones LW, et al. (2016). Exercise training improves obesity-related lymphatic dysfunction. J Physiol 594, 4267–4282. [PubMed: 26931178]

Ivanov S, Scallan JP, Kim KW, Werth K, Johnson MW, Saunders BT, Wang PL, Kuan EL, Straub AC, Ouhachi M, et al. (2016). CCR7 and IRF4-dependent dendritic cells regulate lymphatic collecting vessel permeability. J Clin Invest 126, 1581–1591. [PubMed: 26999610]

Januzzi JL Jr., Lyass A, Liu Y, Gaggin H, Trebnick A, Maisel AS, D'Agostino RB Sr., Wang TJ, Massaro J, and Vasan RS (2016). Circulating Proneurotensin Concentrations and Cardiovascular Disease Events in the Community: The Framingham Heart Study. Arterioscler Thromb Vasc Biol 36, 1692–1697. [PubMed: 27312221]

Johnson LA, and Jackson DG (2010). Inflammation-induced secretion of CCL21 in lymphatic endothelium is a key regulator of integrin-mediated dendritic cell transmigration. Int Immunol 22, 839–849. [PubMed: 20739459]

Johnson LA, and Jackson DG (2013). The chemokine CX3CL1 promotes trafficking of dendritic cells through inflamed lymphatics. J Cell Sci 126, 5259–5270. [PubMed: 24006262]

Kabashima K, Shiraishi N, Sugita K, Mori T, Onoue A, Kobayashi M, Sakabe J, Yoshiki R, Tamamura H, Fujii N, et al. (2007). CXCL12-CXCR4 engagement is required for migration of cutaneous dendritic cells. Am J Pathol 171, 1249–1257. [PubMed: 17823289]

Karkkainen MJ, Saaristo A, Jussila L, Karila KA, Lawrence EC, Pajusola K, Bueler H, Eichmann A, Kauppinen R, Kettunen MI, et al. (2001). A model for gene therapy of human hereditary lymphedema. Proc Natl Acad Sci U S A 98, 12677–12682. [PubMed: 11592985]

Kim ER, Leckstrom A, and Mizuno TM (2008). Impaired anorectic effect of leptin in neurotensin receptor 1-deficient mice. Behav Brain Res 194, 66–71. [PubMed: 18639588]

Kleczkowska P, and Lipkowski AW (2013). Neurotensin and neurotensin receptors: characteristic, structure-activity relationship and pain modulation--a review. Eur J Pharmacol 716, 54–60. [PubMed: 23500196]

Koon HW, Kim YS, Xu H, Kumar A, Zhao D, Karagiannides I, Dobner PR, and Pothoulakis C (2009). Neurotensin induces IL-6 secretion in mouse preadipocytes and adipose tissues during 2,4,6,-trinitrobenzensulphonic acid-induced colitis. Proc Natl Acad Sci U S A 106, 8766–8771. [PubMed: 19443690]

Kuan EL, Ivanov S, Bridenbaugh EA, Victora G, Wang W, Childs EW, Platt AM, Jakubzick CV, Mason RJ, Gashev AA, et al. (2015). Collecting lymphatic vessel permeability facilitates adipose tissue inflammation and distribution of antigen to lymph node-homing adipose tissue dendritic cells. J Immunol 194, 5200–5210. [PubMed: 25917096]

Kutschera S, Weber H, Weick A, De Smet F, Genove G, Takemoto M, Prahst C, Riedel M, Mikelis C, Baulande S, et al. (2011). Differential endothelial transcriptomics identifies semaphorin 3G as a vascular class 3 semaphorin. Arterioscler Thromb Vasc Biol 31, 151–159. [PubMed: 20947821]

Le CP, Nowell CJ, Kim-Fuchs C, Botteri E, Hiller JG, Ismail H, Pimentel MA, Chai MG, Karnezis T, Rotmensz N, et al. (2016). Chronic stress in mice remodels lymph vasculature to promote tumour cell dissemination. Nat Commun 7, 10634. [PubMed: 26925549]

Lee E, Pandey NB, and Popel AS (2014). Lymphatic endothelial cells support tumor growth in breast cancer. Sci Rep 4, 5853. [PubMed: 25068296]

Leinninger GM, Opland DM, Jo YH, Faouzi M, Christensen L, Cappellucci LA, Rhodes CJ, Gnegy ME, Becker JB, Pothos EN, et al. (2011). Leptin action via neurotensin neurons controls orexin,

the mesolimbic dopamine system and energy balance. Cell Metab 14, 313–323. [PubMed: 21907138]

Li J, Song J, Zaytseva YY, Liu Y, Rychahou P, Jiang K, Starr ME, Kim JT, Harris JW, Yiannikouris FB, et al. (2016). An obligatory role for neurotensin in high-fat-diet-induced obesity. Nature 533, 411–415. [PubMed: 27193687]

Li Z, Solomonidis EG, Meloni M, Taylor RS, Duffin R, Dobie R, Magalhaes MS, Henderson BEP, Louwe PA, D'Amico G, et al. (2019). Single-cell transcriptome analyses reveal novel targets modulating cardiac neovascularization by resident endothelial cells following myocardial infarction. Eur Heart J 40, 2507–2520. [PubMed: 31162546]

Lin BZ, Pilch PF, and Kandror KV (1997). Sortilin is a major protein component of Glut4-containing vesicles. J Biol Chem 272, 24145–24147. [PubMed: 9305862]

Liu X, De la Cruz E, Gu X, Balint L, Oxendine-Burns M, Terrones T, Ma W, Kuo HH, Lantz C, Bansal T, et al. (2020). Lymphoangiocrine signals promote cardiac growth and repair. Nature 588, 705–711. [PubMed: 33299187]

Macosko EZ, Basu A, Satija R, Nemesh J, Shekhar K, Goldman M, Tirosh I, Bialas AR, Kamitaki N, Martersteck EM, et al. (2015). Highly Parallel Genome-wide Expression Profiling of Individual Cells Using Nanoliter Droplets. Cell 161, 1202–1214. [PubMed: 26000488]

Madisen L, Zwingman TA, Sunkin SM, Oh SW, Zariwala HA, Gu H, Ng LL, Palmiter RD, Hawrylycz MJ, Jones AR, et al. (2010). A robust and high-throughput Cre reporting and characterization system for the whole mouse brain. Nat Neurosci 13, 133–140. [PubMed: 20023653]

Mazella J, Botto JM, Guillemare E, Coppola T, Sarret P, and Vincent JP (1996). Structure, functional expression, and cerebral localization of the levocabastine-sensitive neurotensin/neuromedin N receptor from mouse brain. J Neurosci 16, 5613–5620. [PubMed: 8795617]

Mazella J, and Vincent JP (2006). Functional roles of the NTS2 and NTS3 receptors. Peptides 27, 2469–2475. [PubMed: 16872720]

Mazella J, Zsurger N, Navarro V, Chabry J, Kaghad M, Caput D, Ferrara P, Vita N, Gully D, Maffrand JP, et al. (1998). The 100-kDa neurotensin receptor is gp95/sortilin, a non-G-protein-coupled receptor. J Biol Chem 273, 26273–26276. [PubMed: 9756851]

McGeown JG, McHale NG, and Thornbury KD (1987). The effect of electrical stimulation of the sympathetic chain on peripheral lymph flow in the anaesthetized sheep. J Physiol 393, 123–133. [PubMed: 3446793]

McHale NG, Roddie IC, and Thornbury KD (1979). Noradrenaline as an excitatory neutrotransmitter in bovine mesenteric lymphatics [proceedings]. J Physiol 295, 94P.

McHale NG, Roddie IC, and Thornbury KD (1980). Nervous modulation of spontaneous contractions in bovine mesenteric lymphatics. J Physiol 309, 461–472. [PubMed: 7252876]

Melander O, Maisel AS, Almgren P, Manjer J, Belting M, Hedblad B, Engstrom G, Kilger U, Nilsson P, Bergmann A, et al. (2012). Plasma proneurotensin and incidence of diabetes, cardiovascular disease, breast cancer, and mortality. JAMA 308, 1469–1475. [PubMed: 23047361]

Mendoza A, Fang V, Chen C, Serasinghe M, Verma A, Muller J, Chaluvadi VS, Dustin ML, Hla T, Elemento O, et al. (2017). Lymphatic endothelial S1P promotes mitochondrial function and survival in naive T cells. Nature 546, 158–161. [PubMed: 28538737]

Moore TC (1984). Modification of lymphocyte traffic by vasoactive neurotransmitter substances. Immunology 52, 511–518. [PubMed: 6146565]

Morris NJ, Ross SA, Lane WS, Moestrup SK, Petersen CM, Keller SR, and Lienhard GE (1998). Sortilin is the major 110-kDa protein in GLUT4 vesicles from adipocytes. J Biol Chem 273, 3582–3587. [PubMed: 9452485]

Munck Petersen C, Nielsen MS, Jacobsen C, Tauris J, Jacobsen L, Gliemann J, Moestrup SK, and Madsen P (1999). Propeptide cleavage conditions sortilin/neurotensin receptor-3 for ligand binding. EMBO J 18, 595–604. [PubMed: 9927419]

Nitti MD, Hespe GE, Kataru RP, Garcia Nores GD, Savetsky IL, Torrisi JS, Gardenier JC, Dannenberg AJ, and Mehrara BJ (2016). Obesity-induced lymphatic dysfunction is reversible with weight loss. J Physiol 594, 7073–7087. [PubMed: 27619475]

Oliver G, Kipnis J, Randolph GJ, and Harvey NL (2020). The Lymphatic Vasculature in the 21(st) Century: Novel Functional Roles in Homeostasis and Disease. Cell 182, 270–296. [PubMed: 32707093]

Petrova TV, and Koh GY (2020). Biological functions of lymphatic vessels. Science 369.

Porras A, Alvarez AM, Valladares A, and Benito M (1998). p42/p44 mitogen-activated protein kinases activation is required for the insulin-like growth factor-I/insulin induced proliferation, but inhibits differentiation, in rat fetal brown adipocytes. Mol Endocrinol 12, 825–834. [PubMed: 9626658]

Quistgaard EM, Madsen P, Groftehauge MK, Nissen P, Petersen CM, and Thirup SS (2009). Ligands bind to Sortilin in the tunnel of a ten-bladed beta-propeller domain. Nat Struct Mol Biol 16, 96–98. [PubMed: 19122660]

Randolph GJ, Bala S, Rahier JF, Johnson MW, Wang PL, Nalbantoglu I, Dubuquoy L, Chau A, Pariente B, Kartheuser A, et al. (2016). Lymphoid Aggregates Remodel Lymphatic Collecting Vessels that Serve Mesenteric Lymph Nodes in Crohn Disease. Am J Pathol 186, 3066–3073. [PubMed: 27746181]

Randolph GJ, Ivanov S, Zinselmeyer BH, and Scallan JP (2017). The Lymphatic System: Integral Roles in Immunity. Annu Rev Immunol 35, 31–52. [PubMed: 27860528]

Ratner C, He Z, Grunddal KV, Skov LJ, Hartmann B, Zhang F, Feuchtinger A, Bjerregaard A, Christoffersen C, Tschop MH, et al. (2019). Long-Acting Neurotensin Synergizes With Liraglutide to Reverse Obesity Through a Melanocortin-Dependent Pathway. Diabetes 68, 1329–1340. [PubMed: 30936142]

Ratner C, Skov LJ, Raida Z, Bachler T, Bellmann-Sickert K, Le Foll C, Sivertsen B, Dalboge LS, Hartmann B, Beck-Sickinger AG, et al. (2016). Effects of Peripheral Neurotensin on Appetite Regulation and Its Role in Gastric Bypass Surgery. Endocrinology 157, 3482–3492. [PubMed: 27580810]

Remaury A, Vita N, Gendreau S, Jung M, Arnone M, Poncelet M, Culouscou JM, Le Fur G, Soubrie P, Caput D, et al. (2002). Targeted inactivation of the neurotensin type 1 receptor reveals its role in body temperature control and feeding behavior but not in analgesia. Brain Res 953, 63–72. [PubMed: 12384239]

Richard F, Barroso S, Martinez J, Labbe-Jullie C, and Kitabgi P (2001). Agonism, inverse agonism, and neutral antagonism at the constitutively active human neurotensin receptor 2. Mol Pharmacol 60, 1392–1398. [PubMed: 11723247]

Robidoux J, Cao W, Quan H, Daniel KW, Moukdar F, Bai X, Floering LM, and Collins S (2005). Selective activation of mitogen-activated protein (MAP) kinase kinase 3 and p38alpha MAP kinase is essential for cyclic AMP-dependent UCP1 expression in adipocytes. Mol Cell Biol 25, 5466–5479. [PubMed: 15964803]

Roh HC, Tsai LT, Lyubetskaya A, Tenen D, Kumari M, and Rosen ED (2017). Simultaneous Transcriptional and Epigenomic Profiling from Specific Cell Types within Heterogeneous Tissues In Vivo. Cell Rep 18, 1048–1061. [PubMed: 28122230]

Roh HC, Tsai LTY, Shao M, Tenen D, Shen Y, Kumari M, Lyubetskaya A, Jacobs C, Dawes B, Gupta RK, et al. (2018). Warming Induces Significant Reprogramming of Beige, but Not Brown, Adipocyte Cellular Identity. Cell Metab 27, 1121–1137 e1125. [PubMed: 29657031]

Rosen ED (2002). The molecular control of adipogenesis, with special reference to lymphatic pathology. Ann N Y Acad Sci 979, 143–158; discussion 188-196. [PubMed: 12543724]

Russell JA, Zimmerman K, and Middendorf WF (1980). Evidence for alpha-adrenergic innervation of the isolated canine thoracic duct. J Appl Physiol Respir Environ Exerc Physiol 49, 1010–1015. [PubMed: 6254935]

Rutkowski JM, Markhus CE, Gyenge CC, Alitalo K, Wiig H, and Swartz MA (2010). Dermal collagen and lipid deposition correlate with tissue swelling and hydraulic conductivity in murine primary lymphedema. Am J Pathol 176, 1122–1129. [PubMed: 20110415]

Sarret P, Gendron L, Kilian P, Nguyen HM, Gallo-Payet N, Payet MD, and Beaudet A (2002). Pharmacology and functional properties of NTS2 neurotensin receptors in cerebellar granule cells. J Biol Chem 277, 36233–36243. [PubMed: 12084713]

Savetsky IL, Torrisi JS, Cuzzone DA, Ghanta S, Albano NJ, Gardenier JC, Joseph WJ, and Mehrara BJ (2014). Obesity increases inflammation and impairs lymphatic function in a mouse model of lymphedema. Am J Physiol Heart Circ Physiol 307, H165–172. [PubMed: 24858842]

Souaze F, Dupouy S, Viardot-Foucault V, Bruyneel E, Attoub S, Gespach C, Gompel A, and Forgez P (2006). Expression of neurotensin and NT1 receptor in human breast cancer: a potential role in tumor progression. Cancer Res 66, 6243–6249. [PubMed: 16778199]

Stan RV, Tse D, Deharvengt SJ, Smits NC, Xu Y, Luciano MR, McGarry CL, Buitendijk M, Nemani KV, Elgueta R, et al. (2012). The diaphragms of fenestrated endothelia: gatekeepers of vascular permeability and blood composition. Dev Cell 23, 1203–1218. [PubMed: 23237953]

Steele FF 3rd, Whitehouse SC, Aday JS, and Prus AJ (2017). Neurotensin NTS1 and NTS2 receptor agonists produce anxiolytic-like effects in the 22-kHz ultrasonic vocalization model in rats. Brain Res 1658, 31–35. [PubMed: 28089664]

Stuart T, Butler A, Hoffman P, Hafemeister C, Papalexi E, Mauck WM 3rd, Hao Y, Stoeckius M, Smibert P, and Satija R (2019). Comprehensive Integration of Single-Cell Data. Cell 177, 1888–1902 e1821. [PubMed: 31178118]

Su ZJ, Liu XY, Zhang JH, Ke SY, and Fei HJ (2019). Neurotensin promotes cholangiocarcinoma metastasis via the EGFR/AKT pathway. Gene 687, 143–150. [PubMed: 30359740]

Swenson KK, Nissen MJ, Leach JW, and Post-White J (2009). Case-control study to evaluate predictors of lymphedema after breast cancer surgery. Oncol Nurs Forum 36, 185–193. [PubMed: 19273407]

Tabarean IV (2020). Neurotensin induces hypothermia by activating both neuronal neurotensin receptor 1 and astrocytic neurotensin receptor 2 in the median preoptic nucleus. Neuropharmacology 171, 108069. [PubMed: 32275927]

Tavakkolizadeh A, Wolfe KQ, and Kangesu L (2001). Cutaneous lymphatic malformation with secondary fat hypertrophy. Br J Plast Surg 54, 367–369. [PubMed: 11355999]

Thomas JB, Giddings AM, Wiethe RW, Olepu S, Warner KR, Sarret P, Gendron L, Longpre JM, Zhang Y, Runyon SP, et al. (2014). Identification of N-[(5-{[(4-methylphenyl)sulfonyl]amino}-3-(trifluoroacetyl)-1H-indol-1-yl)acetyl] -l-leucine (NTRC-824), a neurotensin-like nonpeptide compound selective for the neurotensin receptor type 2. J Med Chem 57, 7472–7477. [PubMed: 25157640]

Thomas JB, Vivancos M, Giddings AM, Wiethe RW, Warner KR, Murza A, Besserer-Offroy E, Longpre JM, Runyon SP, Decker AM, et al. (2016). Identification of 2-({[1-(4-Fluorophenyl)-5-(2-methoxyphenyl)-1H-pyrazol-3-yl]carbonyl}amino)tricyc lo[3.3.1.13,7]decane-2-carboxylic Acid (NTRC-844) as a Selective Antagonist for the Rat Neurotensin Receptor Type 2. ACS Chem Neurosci 7, 1225–1231. [PubMed: 27359371]

Toth F, Mallareddy JR, Tourwe D, Lipkowski AW, Bujalska-Zadrozny M, Benyhe S, Ballet S, Toth G, and Kleczkowska P (2016). Synthesis and binding characteristics of [(3)H]neuromedin N, a NTS2 receptor ligand. Neuropeptides 57, 15–20. [PubMed: 26707235]

Tyler-McMahon BM, Boules M, and Richelson E (2000). Neurotensin: peptide for the next millennium. Regul Pept 93, 125–136. [PubMed: 11033059]

Valladares A, Roncero C, Benito M, and Porras A (2001). TNF-alpha inhibits UCP-1 expression in brown adipocytes via ERKs. Opposite effect of p38MAPK. FEBS Lett 493, 6–11. [PubMed: 11277995]

Vanlandewijck M, He L, Mae MA, Andrae J, Ando K, Del Gaudio F, Nahar K, Lebouvier T, Lavina B, Gouveia L, et al. (2018). A molecular atlas of cell types and zonation in the brain vasculature. Nature 554, 475–480. [PubMed: 29443965]

Vita N, Oury-Donat F, Chalon P, Guillemot M, Kaghad M, Bachy A, Thurneyssen O, Garcia S, Poinot-Chazel C, Casellas P, et al. (1998). Neurotensin is an antagonist of the human neurotensin NT2 receptor expressed in Chinese hamster ovary cells. Eur J Pharmacol 360, 265–272. [PubMed: 9851594]

Wang JG, Li NN, Li HN, Cui L, and Wang P (2011). Pancreatic cancer bears overexpression of neurotensin and neurotensin receptor subtype-1 and SR 48692 counteracts neurotensin induced cell proliferation in human pancreatic ductal carcinoma cell line PANC-1. Neuropeptides 45, 151–156. [PubMed: 21272935]

Weitman ES, Aschen SZ, Farias-Eisner G, Albano N, Cuzzone DA, Ghanta S, Zampell JC, Thorek D, and Mehrara BJ (2013). Obesity impairs lymphatic fluid transport and dendritic cell migration to lymph nodes. PLoS One 8, e70703. [PubMed: 23950984]

Wolock SL, Lopez R, and Klein AM (2019). Scrublet: Computational Identification of Cell Doublets in Single-Cell Transcriptomic Data. Cell Syst 8, 281–291 e289. [PubMed: 30954476]

Woodworth HL, Beekly BG, Batchelor HM, Bugescu R, Perez-Bonilla P, Schroeder LE, and Leinninger GM (2017). Lateral Hypothalamic Neurotensin Neurons Orchestrate Dual Weight Loss Behaviors via Distinct Mechanisms. Cell Rep 21, 3116–3128. [PubMed: 29241540]

Zeng W, Pirzgalska RM, Pereira MM, Kubasova N, Barateiro A, Seixas E, Lu YH, Kozlova A, Voss H, Martins GG, et al. (2015). Sympathetic neuro-adipose connections mediate leptin-driven lipolysis. Cell 163, 84–94. [PubMed: 26406372]

Zeng X, Ye M, Resch JM, Jedrychowski MP, Hu B, Lowell BB, Ginty DD, and Spiegelman BM (2019). Innervation of thermogenic adipose tissue via a calsyntenin 3beta-S100b axis. Nature 569, 229–235. [PubMed: 31043739]

Zhang F, Zarkada G, Han J, Li J, Dubrac A, Ola R, Genet G, Boye K, Michon P, Kunzel SE, et al. (2018). Lacteal junction zippering protects against diet-induced obesity. Science 361, 599–603. [PubMed: 30093598]

Zhao Q, Eichten A, Parveen A, Adler C, Huang Y, Wang W, Ding Y, Adler A, Nevins T, Ni M, et al. (2018). Single-Cell Transcriptome Analyses Reveal Endothelial Cell Heterogeneity in Tumors and Changes following Antiangiogenic Treatment. Cancer Res 78, 2370–2382. [PubMed: 29449267]

Zhuo W, Jia L, Song N, Lu XA, Ding Y, Wang X, Song X, Fu Y, and Luo Y (2012). The CXCL12-CXCR4 chemokine pathway: a novel axis regulates lymphangiogenesis. Clin Cancer Res 18, 5387–5398. [PubMed: 22932666]

Highlights

1. *Nts*, which encodes neurotensin, is expressed by lymphatic endothelial cells (LECs)
2. *Nts* expression in BAT-localized LECs is inhibited by adrenergic signaling
3. Neurotensin represses thermogenesis in brown adipocytes via NTSR2 and ERK signaling
4. Knockout of *Nts* or NTSR2 inhibition *in vivo* enhanced cold tolerance in mice

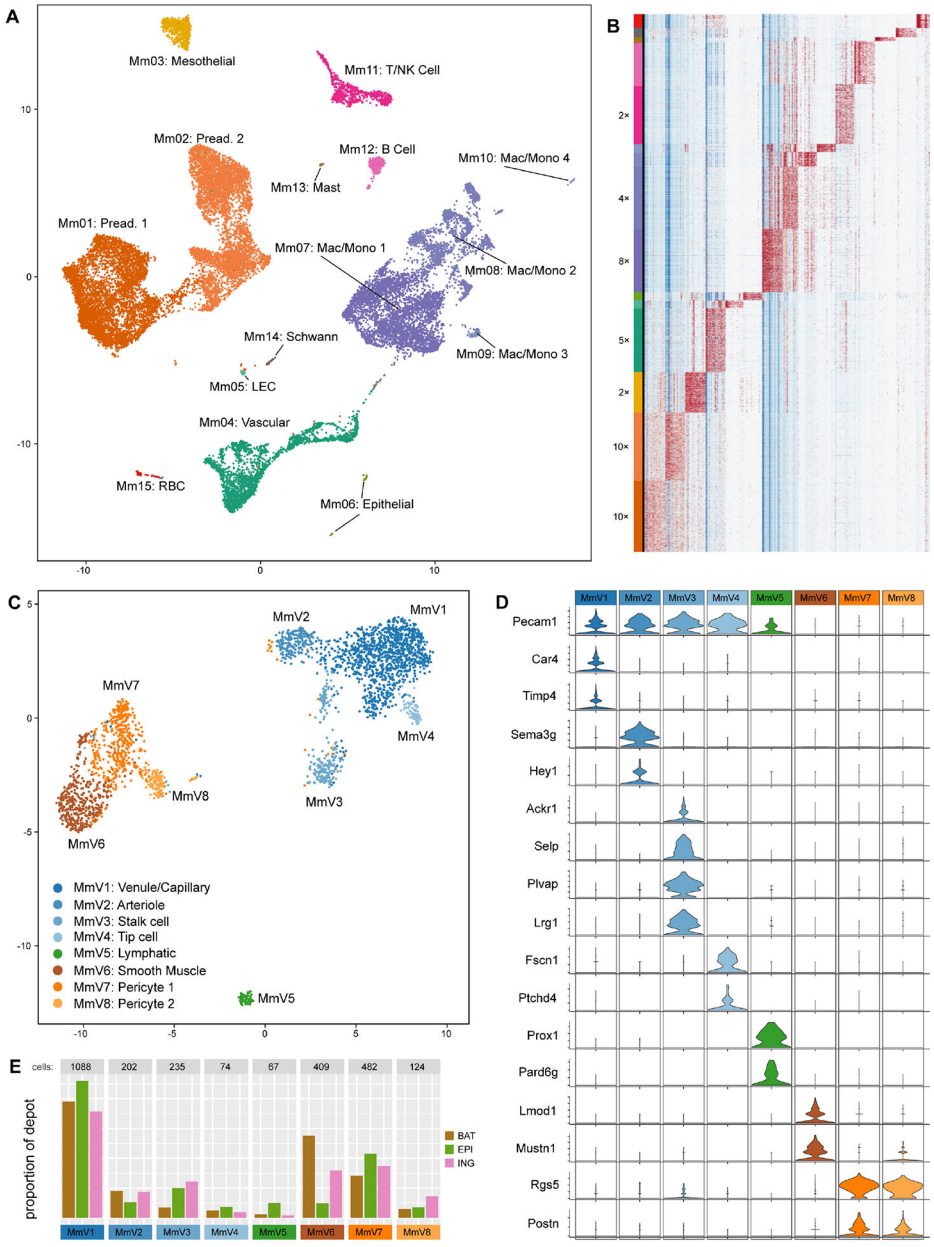

Figure 1. Major cell types of mouse whole SVF and vascular fraction shared across 3 depots.

(A) UMAP plot of ~23,000 cells collected from mouse SVF across 3 depots: eWAT, iWAT, and BAT.

(B) Expression heatmap of the top 10 marker genes from each cluster (columns), ordered by cell (rows) and grouped by cluster (left-most color bar); the largest clusters were downsampled (factor shown to the left of the cluster bar) so that smaller clusters are visible at the scale shown.

(C) UMAP plot of 2681 mouse vascular cells – clusters “Mm04” and “Mm05” from (A).

(D) Violin plots of highly-specific marker genes for the clusters shown in (C); *Pecam1* is also shown as a general marker for endothelial cells, including the lymphatic endothelial population.

(E) Breakdown of the origin of the cells comprising each cluster in (C); the y-axis shows the proportion of cells belonging to each depot (color) that belong to each cluster (x-axis).

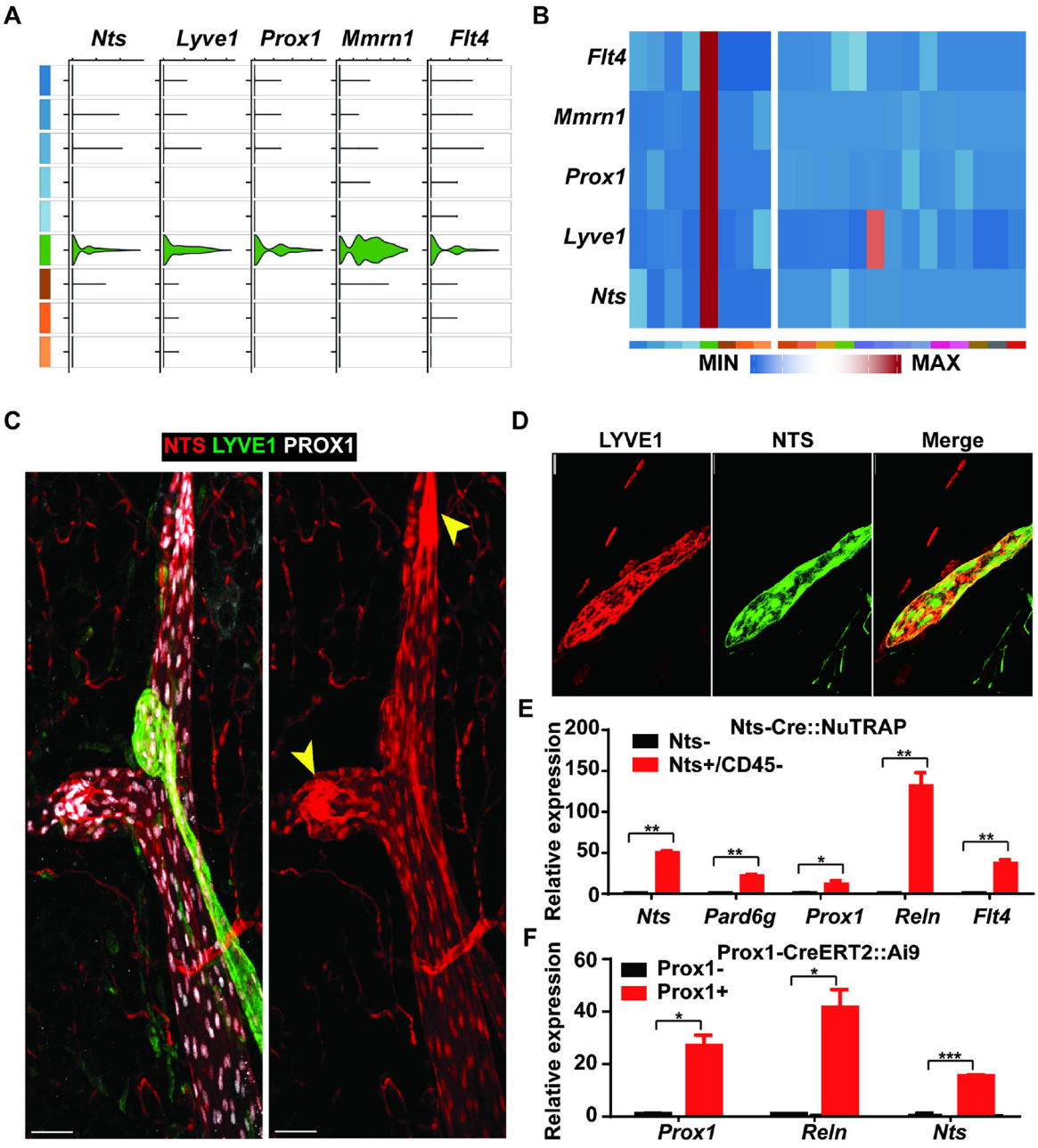

Figure 2. Nts is expressed by adipose LECs.

(A) Violin plot showing co-expression of *Nts* with canonical lymphatic endothelial maker genes *Lyve1, Prox1, Mmrn1*, and *Flt4*.

(B) Heatmaps of average RNA expression for these genes in the mouse vascular clusters (left panel) and all other mouse SVF clusters (right panel). Expression levels are normalized by row.

(C) Representative image of LVs from mesenteric fat of an NTS-Cre::Ai9 mouse ($n = 15$ images from 5 mice). Prox1 (white) marks LVs. High expression of Lyve-1 (green) indicates a lymphatic capillary. tdTomato (red) marks expression of NTS-Cre, present in both

lymphatic capillaries and collecting ducts. Yellow arrowheads indicate valves within collecting lymphatics. Scale bar, 50 μm.

(D) Representative image of lymphatic capillary from mesenteric fat of an NTS-Cre::Ai9 mouse. tdTomato (green) marks expression of NTS-Cre, with counterstaining with anti-Lyve-1 (red) (n= 15 images from 5 mice). Scale bar, 25 μm.

(E) Expression of *Nts* and lymphatic marker genes in NTS+ and NTS− cells isolated from the eWAT SVF of NTS-Cre::NuTRAP mice. n = 2; Mean ± SD. *P < 0.05, **P < 0.01

(F) Expression of *Nts* and lymphatic marker genes in Prox1+ and Prox1− cells isolated from the eWAT SVF of Prox1-CreERT2::Ai9 mice. n = 2; Mean ± SD. *P < 0.05, ***P < 0.001

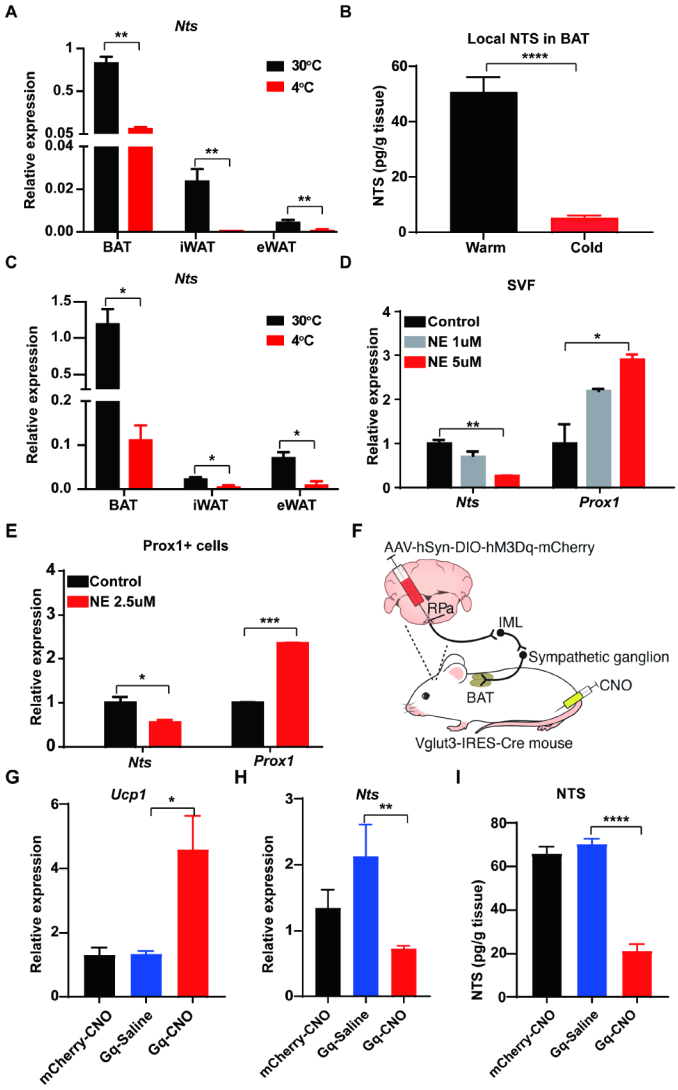

Figure 3. *Nts* expression in BAT LECs is repressed by cold exposure and sympathetic activation.

(A) Expression of *Nts* mRNA in the SVF of BAT, eWAT, and iWAT of mice housed at 30°C and 4°C. $n = 5$; Mean ± SD. $^{**}P < 0.01$

(B) NTS protein levels in BAT of mice housed at 30°C or exposed to 4°C for 1 day. $n = 4$-8; Mean ± SD. $^{****}P < 0.0001$.

(C) Expression of *Nts* in Prox1+ LECs isolated from BAT, eWAT, and iWAT of mice housed at 30°C and 4°C. $n = 5$; Mean ± SD. $^{*}P < 0.05$

(D) Expression of *Nts* and *Prox1* in the SVF cells of BAT treated *ex vivo* with norepinephrine. $n = 2$; Mean ± SD. $^{*}P < 0.05$, $^{**}P < 0.01$

(E) Expression of *Nts* and *Prox1* in Prox1+ cells isolated from BAT treated *ex vivo* with norepinephrine. $n = 2$; Mean ± SD. $^{*}P < 0.05$, $^{***}P < 0.001$

(F) Schematic of experiment testing effect of chemogenetic activation of glutamatergic neurons in the raphe pallidus (RPa). AAV2/8-hSyn-DIO-hM3Dq-mCherry virus (or mCherry only) was injected into the RPa of Vglut3-IRES-Cre mice, resulting in specific expression of the DREADD hM3Dq in the glutamatergic neurons upstream of the

sympathetic outflow tract. Administration of CNO activates the DREADD, promoting activation of the SNS from the RPa, through the intermediolateral nucleus of the spinal cord (IML), and then the sympathetic nerves to BAT.

(G) Expression of *Ucp1* mRNA in BAT in mice from (F) treated with CNO or vehicle. n = 3-5; Mean ± SD. $^{*}P < 0.05$.

(H) Expression of *Nts* mRNA in BAT in mice from (F) treated with CNO or vehicle. n = 3-5; Mean ± SD. $^{*}P < 0.05$.

(I) NTS protein levels in BAT in mice from (F) treated with CNO or vehicle. n = 3-5; Mean ± SD. $^{***}P < 0.001$.

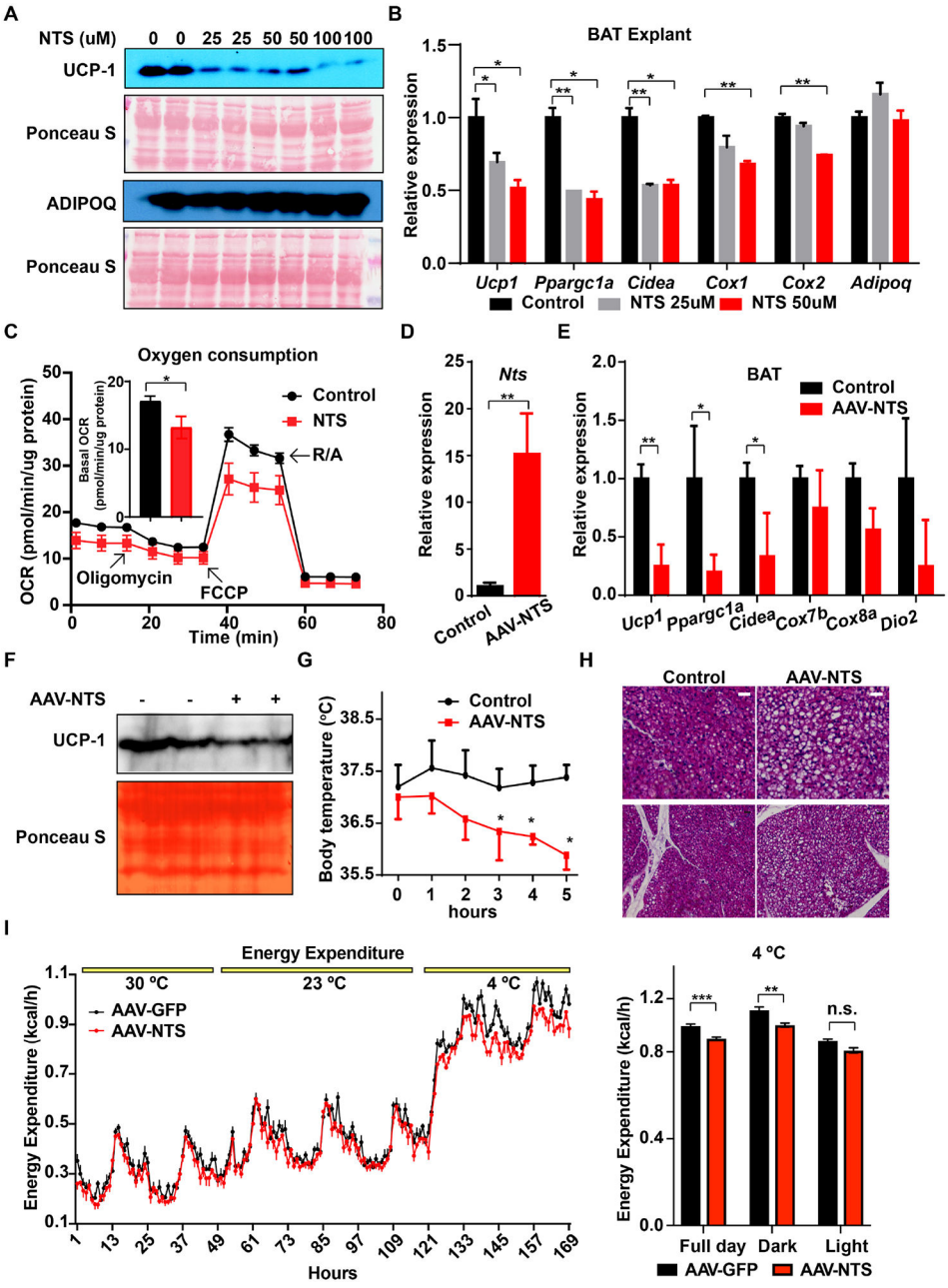

Figure 4. Exogenous NTS reduces adipose thermogenesis.

(A) BAT explants were exposed to the indicated concentration of NTS for 24 hours prior to harvest and Western blotting. Representative image from three Western blots.

(B) qRT-PCR analysis of BAT explants treated as in (A). $n = 2$; Mean ± SD. $*P < 0.05$, $***P < 0.001$

(C) Oxygen consumption rate (OCR) in cultured brown adipocytes treated with NTS (25 uM) for 16 hrs. Inset shows basal OCR over the first 15 min. $n = 13$; Mean ± SD. $*P < 0.05$. Two technical repeats performed.

(D) Expression of *Nts* in BAT after direct delivery of AAV-Nts (vs. control AAV) for three weeks. $n = 5$; Mean ± SD. $**P < 0.01$

(E) Expression of thermogenic genes in BAT after direct delivery of AAV-Nts (vs. control AAV). $n = 5$; Mean ± SD. $*P < 0.05$, $**P < 0.01$

(F) UCP-1 protein expression in BAT three weeks after direct delivery of AAV-Nts (vs. control AAV). Representative image from two Western blots.

(G) Rectal temperature of mice exposed to 4°C three weeks after direct delivery of AAV-Nts or a control AAV. Mice were initially housed at 23°C. $n = 5$; Mean ± SD. $*P < 0.05$

(H) BAT histology three weeks after direct delivery of AAV-Nts (vs. control AAV) at room temperature. Representative image from ($n = 5$ images from 5 mice).

(I) Indirect calorimetry of mice treated with AAV-NTS or control AAV at 30°C, 23°C, and 4°C. Data were normalized to lean body mass and analyzed by ANCOVA.

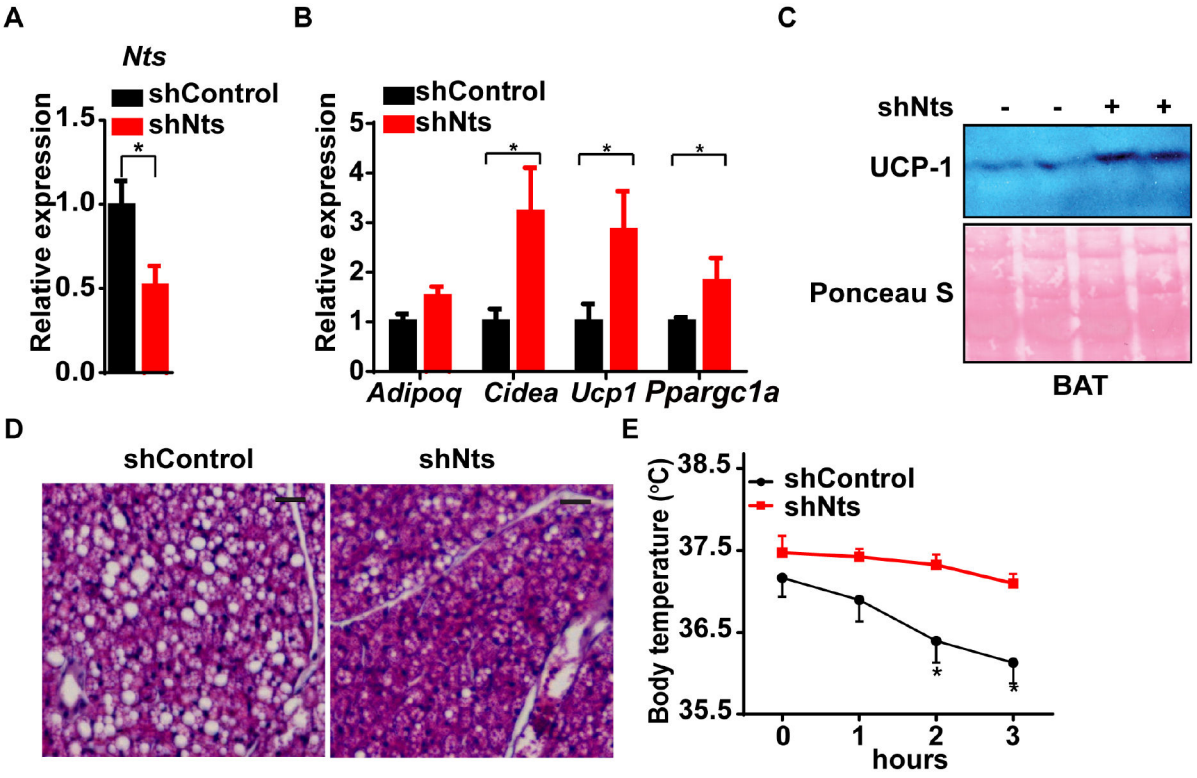

Figure 5. Loss of NTS induces thermogenesis in BAT.

(A) Expression of *Nts* in BAT after direct AAV delivery of shNts or a control shRNA for three weeks. $n = 5$; Mean ± SD.

(B) Expression of thermogenic genes in BAT after direct delivery of AAV-shNts or a control shRNA for three weeks. $n = 5$; Mean ± SD.

(C) UCP-1 protein expression in BAT three weeks after direct delivery of AAV-shNts (vs. shControl). Representative image from two Western blots.

(D) BAT histology three weeks after direct delivery of AAV-shNts (vs. shControl) at 30°C. Representative image from ($n = 5$ images from 5 mice).

(E) Rectal temperature of mice exposed to 4°C three weeks after direct delivery of AAV-shNts or a control shRNA. Mice were initially housed at 30°C. $n = 5$; Mean ± SD.

*$P < 0.05$ for all panels

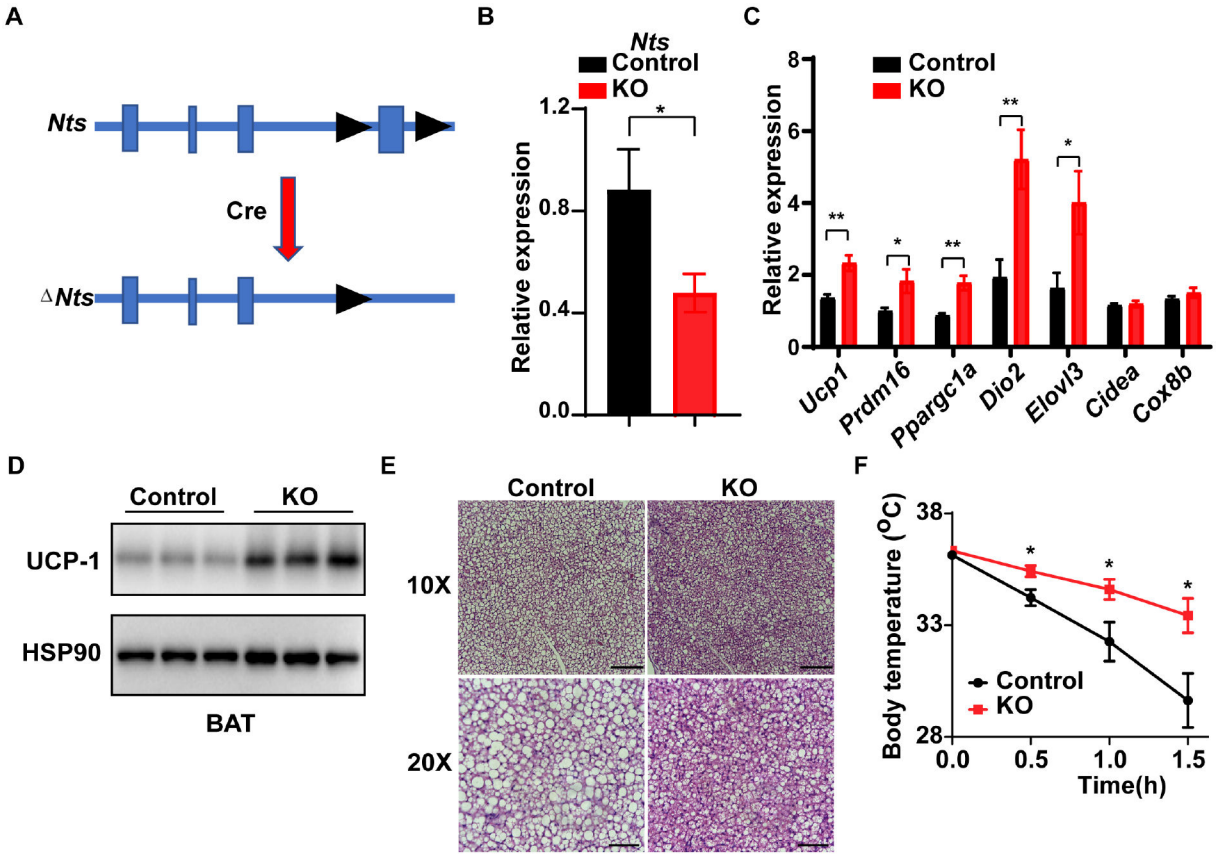

Figure 6. Conditional deletion of *Nts* in LECs causes increased thermogenic gene expression and cold tolerance.

(A) Scheme of the floxed *Nts* allele. Exon 4 contains the complete protein sequence of NTS.

(B) Crossing Nts^{flox} mice to Prox1-CreERT2 mice and treating with tamoxifen (2 mg IP for 11 days) causes reduced *Nts* mRNA expression in BAT. Control animals are Nts^{flox} mice without Cre, also treated with tamoxifen. $n = 6$; Mean ± SD. $^{*}P < 0.05$.

(C) Expression of thermogenic genes in BAT after tamoxifen-mediated knockout of *Nts* (compared to Nts^{flox} mice without Cre, also treated with tamoxifen). $n = 6$; Mean ± SD. $^{*}P < 0.05$, $^{**}P < 0.01$

(D) UCP-1 protein levels in BAT in Ly-NTSKO mice. Representative image from two Western blots.

(E) BAT histology in Ly-NTSKO and control mice at 30°C. Representative image from ($n =$ 3 images from 3 mice).

(F) Rectal temperature of Ly-NTSKO and control mice exposed to 6°C. Mice were initially housed at 30°C. $n = 5$; Mean ± SD.

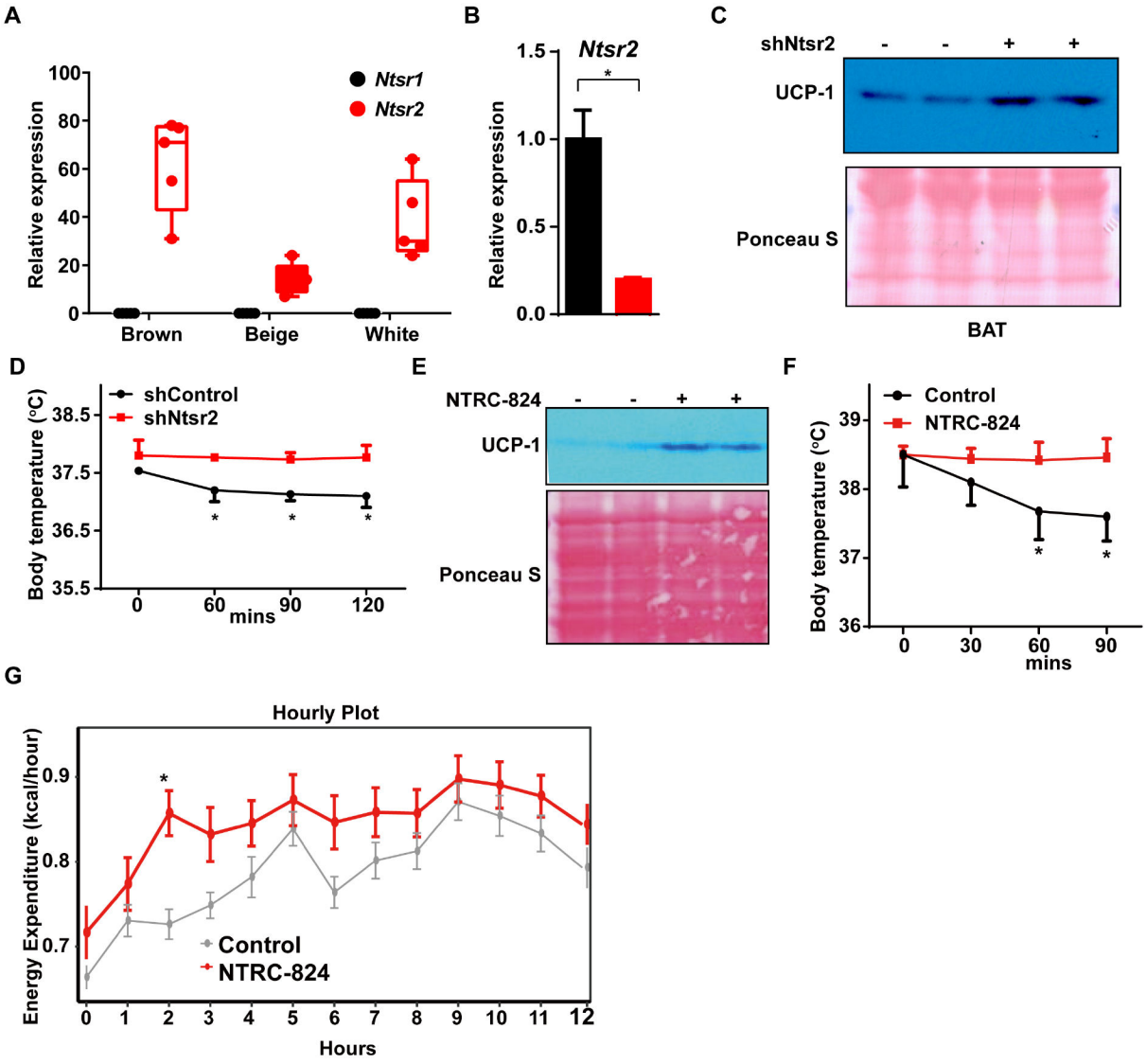

Figure 7. NTSR2 is the major target of NTS in thermogenic adipocytes.

(A) Expression of *Ntsr1* and *Ntsr2* in RNA-seq data from isolated brown, beige, and white adipocytes.

(B) Expression of *Ntsr2* in BAT after direct delivery of AAV-shNtsr2 or a control shRNA three weeks. $n = 5$; Mean ± SD. $^*P < 0.05$

(C) UCP-1 protein expression in BAT three weeks after injection of AAV-shNtsr2 (vs. shControl). Representative image from two Western blots.

(D) Rectal temperature of mice exposed to 4°C 2 weeks after direct delivery of AAV-shNtsr2 or a control shRNA. Mice were initially housed at 30°C. $n = 5$; Mean ± SD.

(E) 8-week-old lean male mice received intraperitoneal (IP) injections of NTRC-824 (5 mg/kg) or DMSO while housed at 30°C. UCP-1 protein expression in BAT is shown three weeks after injection of NTRC-824 or vehicle. Representative image from two Western blots.

(F) Rectal temperature of mice exposed to 4°C 2 weeks after treatment with NTRC-824 (5 mg/kg) or vehicle. Mice were initially housed at 30°C. $n = 5$; Mean ± SD.
(G) Energy expenditure as measured by indirect calorimetry. Mice were treated as in (E) before placement in CLAMS unit. Data are normalized to lean body mass. $n = 6\text{-}7$; Mean ± SD. $*P < 0.05$

KEY RESOURCES TABLE

REAGENT or RESOURCE	SOURCE	IDENTIFIER
Antibodies		
anti-GFP	Novus	NB-100-1678
anti-LYVE1	Abcam	ab14917
anti-HSP90	Cell signaling technology	4874S
anti-mCherry	Thermo Fisher	M11217
anti-CD31	BD Bioscience	550274
anti-TH	Millipore	AB152
anti-c-Fos	Abcam	AB214672
anti-UCP1	Abcam	ab10983
anti-Adipoq	Thermo Fisher	PA1-054
anti-pERK	CST	9106S
anti-ERK	CST	4695
anti-NTS	LifeSpan Biosciences	LS-C400910-20
anti-PROX1	Proteintech	11067-2-AP
Bacterial and Virus Strains		
NTS OE AAV Virus	Applied Biological Materials	AAVP0154993
NTS KD AAV Virus	Applied Biological Materials	iAAV04443008
NTSR2 KD AAV Virus	Applied Biological Materials	iAAV03612808
DREADD AAV Virus	Krashes et al. 2011	N.A.
Biological Samples		
Human adipose SVF	This paper	N.A.
Human lymphatic endothelial cells	This paper	N.A.
Chemicals, Peptides, and Recombinant Proteins		
Neurotensin	Sigma	N6383-10MG
NTRC-824	R&D Systems	5438/50
Neuromedin N	Medchemexpress	HY-P0079
PD 98059	Cayman Chemical	167869-21-8
Collagenase	Worthington Biochemical	LS004196
Norepinephrine	Sigma-Aldrich	A0937-1G
Phentolamine	Sigma-Aldrich	P7547-100MG
Propranolol	Sigma-Aldrich	P8688-100MG
Phenylephrine	Sigma-Aldrich	P6126-5G
Dexmedetomidine	Sigma-Aldrich	SML0956-10MG
Tamoxifen	Sigma-Aldrich	T5648
Clozapine-N-Oxide (CNO)	Sigma-Aldrich	C0832
Methyl Salicylate	Sigma-Aldrich	M6752
Critical Commercial Assays		

REAGENT or RESOURCE	SOURCE	IDENTIFIER
Neurotensin EIA kit	Phoenix Pharmaceuticals	EK-048-03
Deposited Data		
Human and Mouse Adipose SVF Drop-seq data set	Single cell atlas portal	https://singlecell.broadinstitute.org/single_cell/study/SCP133/human-adipose-svf-single-cell
Experimental Models: Cell Lines		
Experimental Models: Organisms/Strains		
C57 B6/J mouse	JAX	000664
$Nts^{flox/flox}$ mouse	This paper	N.A.
Obese C57 B6/J mouse	JAX	380050
NuTRAP mouse	JAX	029899
Ai9(RCL-tdT) mouse	JAX	007909
RC::L-hM3Dq mouse	JAX	026943
NTS-Cre mouse	JAX	017525
Vglut3-Cre mouse	Zeng et al. 2019	N.A.
Prox1-Cre-ERT2 mouse	JAX	022075
Oligonucleotides		
Primers for *Nts, Ntsr2, Prox1, Flt4, Pard6g, Reln, Ucp1, Pgc1a, Adipoq, Cidea, Cox7b, Cox8a, Dio2* in Supplementary Table 1	This paper	N.A.
Recombinant DNA		
Software and Algorithms		
STAR v2.6.1e	https://github.com/alexdobin/STAR	N.A.
Scrublet	Wolock et al., 2019	N.A.
Seurat program (v3.0.3.9036)	Stuart et al., 2019	N.A.
SCTransform	Hafemeister and Satija, 2019	N.A.
Imaris software version 8.4	Bitplane	N.A.
UMAP	Becht et al., 2018	N.A.
Other		